Improved Models for the Potential Energy Functions of the Ground Singlet and Lowest-Lying Triplet States of the Cesium Dimer

by

Jesse Baldwin

A thesis
presented to the University of Waterloo
in fulfillment of the
thesis requirement for the degree of
Master of Science
in
Chemistry

Waterloo, Ontario, Canada, 2012

I hereby declare that I am the sole author of this thesis.

This is a true copy of the thesis, including any required final revisions, as accepted by my examiners.

I understand that my thesis may be made electronically available to the public.

Abstract

The Morse/Long Range (MLR) potential has become one of the most reliable and highly used potential energy functions for diatomic molecules. It includes the theoretical long range behaviour that diatomic molecules are known to exhibit as they approach the dissociation limit. Heavy alkali metals with adjacent electronic states often exhibit strong coupling between the spin and orbital angular momentum. The ground state $X\,^1\Sigma_g^+$ and the lowest lying triplet state $a\,^3\Sigma_u^+$ of Cs_2 exhibit such coupling effects and as a result, modeling the highest vibrational states of these states is a non-trivial problem. Utilizing scattering length values obtained from published analysis of 60 Feshbach resonances, the correct form of the potential energy function was determined. Moreover, the scattering length values were used to determine the correct leading dispersion coefficient that describes the true form of the long-range potential energy functions. All previous attempts to determine global potential energy functions for these states have considered only the optical spectroscopic data. This is the first ever effort attempting to use scattering lengths determined from cold atom collision experiments in a combined analysis with conventional spectroscopic data.

Acknowledgments

I would like to thank my supervisor Dr. Robert J. Le Roy. His optimism has given me both the inspiration and guidance I needed to progress throughout the course of this project. Most importantly, he was always willing to teach and provide insight into what the real physical problems were.

I would like to thank Dr. Frederick R. McCourt. His course instruction was rigourous and demanding, and admittedly, I seldom found sleep during my first four months at the University of Waterloo.

I would also like to express my gratitude to Lee Huntington for his help with troubleshooting a variety of computer problems.

Lastly, I would like to thank my fiance Stefanie for providing the support no other person could have.

To Ray, who continues to be my inspiration.

Contents

List of Figures

List of Tables

List of Abbreviations

BOB - Born-Oppenheimer Breakdown

DPF - Direct-Potential Fit

GMO - Generalized Morse Oscillator

EMO - Extended Morse Oscillator

MLR - Morse/Long-Range

SPP - Spline-Pointwise Potential

PAS - Photoassociation Spectroscopy

MγLR - Morse/Long-Range potential with the first γ terms included in its long-range

Chapter 1

Introduction

The cesium dimer has been receiving increasing attention recently because of interest in cold atom collision phenomena [3, 4, 5]. Particular interest is focused on the two electronic states that are formed from ground state atoms: the ground singlet state $X\,^1\Sigma_g^+$ and the lowest triplet state $a\,^3\Sigma_u^+$, whose potential energy curves are shown schematically in Fig. 1.1. Previous empirical work on these states considered either conventional spectroscopic data for bound vibrational-rotational levels [5, 6, 7], or Feshbach resonances observed in collisional studies of cold atoms [3, 4, 5]. The cesium atom has a nuclear spin angular momentum **I** of magnitude 7/2, spin angular momentum **S** of magnitude 1/2 with two possible orientations, and orbital angular momentum **L** of 0. The total angular momentum **F** is the vector sum of these three individual angular momenta. Thus, atomic cesium has a total angular momentum quantum number F of 3 or 4, depending on the orientation of the electron spin angular momentum vector relative to the nuclear spin angular momentum vector. Studies of the Feshbach resonances of colliding cesium atoms focus on the resonances at collision energies

between the limits where the total angular momenta for atom a and b are $F_a + F_b = 3 + 3$, $3+4$, and $4+4$. The resonances are of particular interest in this work as they define the three most probable asymptotic limits when a cesium dimer breaks apart to yield a pair of ground state Cs atoms. These three asymptotic limits are not statistically equivalent. The average that is weighted by the sum of the degeneracies for the individual energies yields the so-called "hyperfine-free limit" shown schematically in Fig. 1.1 with dash-dot lines. Associated with each of these four limits are s-wave scattering lengths a_s, a property of the continuum wavefunction at zero collision energy. Modelling the potential energy functions of the $X\,^1\Sigma_g^+$ and $a\,^3\Sigma_u^+$ states of Cs_2 by fitting to both the conventional spectroscopic data and to the experimental scattering lengths is the central objective of this work.

The conventional spectroscopic data for this system has been subjected to parameter-fit analyses [8, 6] and to direct-potential fit (DPF) analyses [7, 2], in which transition energy predictions generalized from a parametrized potential function are compared with experiment, and least-squares fitting to minimize discrepancies is used to optimize potential function parameters. The Feshbach resonances were analyzed using a coupled-channel method that yielded estimates of the scattering lengths at the hyperfine-free limit for both the singlet and triplet states [4]. The scattering length is related to the binding energy of the highest bound vibrational level $v_{\max}$, and it is sensitive to the overall well-capacity. In this work, the well-capacity, and hence the binding energy of the highest vibrational levels, are determined by matching the scattering length of an analytical potential defined by a DPF analysis to the values determined by Chin *et al.* [4]. The highest vibrational levels that the analytical potential yield are then compared to those determined using a couple-channel potential that was fitted to the Feshbach resonances [9].

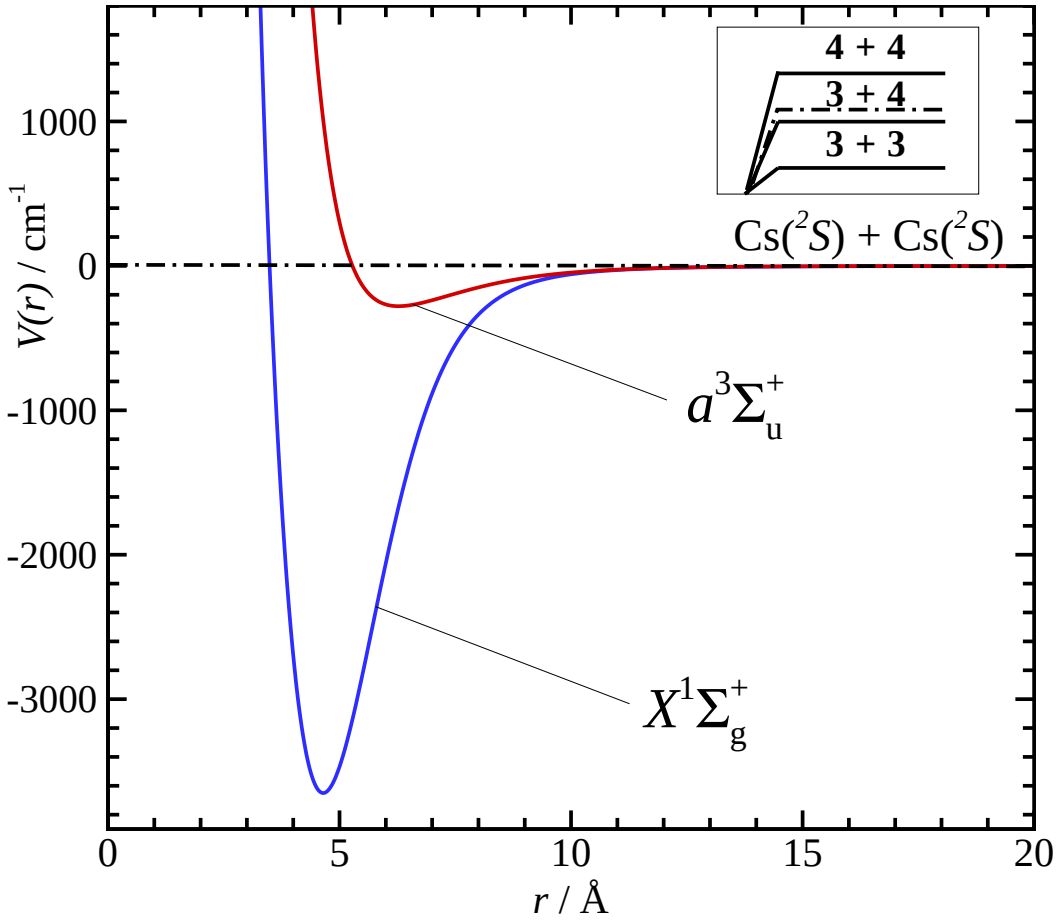

Figure 1.1: Plots of the potentials for the $X\,^1\Sigma_g^+$ and $a\,^3\Sigma_u^+$ states of Cs_2. The horizontal dash-dot lines correspond to the hyperfine-free limit.

Chapter 2 of this document will outline the nature of the computational problem associated with modelling the spectroscopic data for the cesium dimer. In particular, the long-range interaction between two cesium atoms will be described. The direct-potential fit method as it applies to a generalized potential energy function is described, as well as types of commonly used potential energy functions. Lastly, Chapter 2 will describe the data set that the selected potential energy function will be fitted to.

Next, Chapter 3 will outline the techniques by which the parameters of a fitted potential are chosen. Moreover, Chapter 3 explains how the various domains of a potential energy curve are evaluated analytically, and in particular, how the optimal direct-potential fit is obtained, how the extrapolation region or long-range tail is evaluated, and how the potential energy function model may be modified so that its scattering length matches an experimental value using two different potential function parameters, one a physical parameter and the other a non-physical parameter of the model used for the potential energy curve. In addition, the relationship that the singlet-state potential has with the triplet-state potential at long-range will be described and compared to the theoretical model of Vanhaecke *et al.* [3].

Chapter 4 will outline the most recent potential fit that was done on the $X\,^1\Sigma_g^+$ state of the cesium dimer by Coxon and Hajigeorgiou [2], and it will present the potential fit results in the present analysis. Chapter 5 will then outline the previous potential fit work done on the $a\,^3\Sigma_u^+$ state of the cesium dimer by Xie *et al.* [7], and it will present the potential fit results of the present analysis. Chapter 6 will present the implications of the results for the $X\,^1\Sigma_g^+$ and $a\,^3\Sigma_u^+$ states of the cesium dimer.

Chapter 2

Modelling the Potential Energy Curve of Diatomic Molecules

2.1 Long-Range Behaviour of Diatomic Molecules

Molecules exhibit qualities in their long-range interaction that are very distinct, and these forces can be described mathematically. The forces that govern the long-range interaction between S-state atoms are referred to as dispersion forces [10]. All homonuclear diatomic species exhibit dispersion forces that have the same functional form, but differ in the values of the coefficients that determine the strength of the interaction. These interactions are discussed by Margenau [10], who shows that the leading long-range term is proportional to $-1/r^6$. Thus, the basic functional form for dispersion interaction energy of diatomic molecules is:

$$V(r) = -\frac{C_6}{r^6} \tag{2.1}$$

where C_6 is the leading van der Waals coefficient and has a unique value for each molecular system. It was shown through a simplistic derivation that the basic form of the dispersion forces contributing to the potential energy of a diatomic molecule is [10]:

$$V(r) = -\frac{C_6}{r^6} - \frac{C_8}{r^8} - \frac{C_{10}}{r^{10}} + \cdots \tag{2.2}$$

This functional form has been expanded to include higher-order terms $-C_m/r^m$ where $m > 10$ so that the complete representation of the long-range potential interaction derived from second-order perturbation theory is:

$$V(r) = -\sum_{m=6(2)}^{\infty} \frac{C_m}{r^m} \tag{2.3}$$

For interactions between ground-state atoms, all of the terms contributing to the potential energy function are attractive and thus, the associated C_m coefficients are positive.

This functional form has provided an accurate description for the attractive dispersion forces of diatomic molecules. However, there also exists repulsive dispersion forces that arise in third-order perturbation theory. If the second- and third-order terms are included in Eq. (2.2) then the long range expression for the $X\,^1\Sigma_g^+$ and $a\,^3\Sigma_u^+$ states of Cs_2 is:

$$V(r) = \mathfrak{D}_e - \frac{C_6}{r^6} - \frac{C_8}{r^8} - \frac{C_{10}}{r^{10}} + \frac{C_{11}}{r^{11}} - \frac{C_{12}}{r^{12}} + \frac{C_{13}}{r^{13}} - \frac{C_{14}}{r^{14}} \tag{2.4}$$

For the molecular species Cs_2, many groups have worked to determine the long-range potential coefficients [8, 11, 12, 13, 14, 15, 16, 6, 2]. However, optimum values of the higher-

order van der Waals coefficients contributing to the long-range interaction potential of Cs_2 are still uncertain. Tables 2.1 and 2.2 contain all reported values of the second- and third-order dispersion coefficients for the $X\,^1\Sigma_g^+$ and $a\,^3\Sigma_u^+$ states of Cs_2.

Table 2.1: Second-order dispersion coefficients C_m for the $X\,^1\Sigma_g^+$ and $a\,^3\Sigma_u^+$ states of Cs_2 in units of cm^{-1} $Å^m$

Year	Author(s)	$10^{-7}C_6$	$10^{-9}C_8$	$10^{-10}C_{10}$	$10^{-12}C_{12}$	$10^{-14}C_{14}$
1985	Weickenmeier *et al.* [8]	3.298	1.254	5.525	3.07	2.151
1994	Marinescu [11]	3.051	1.300	5.7443		
1997	Patil and Tang [12]	3.206	1.289	5.132	2.677	1.87
1999	Patil and Tang [13]	3.088	1.227	4.924	2.585	
1999	Derevianko *et al.* [14]	3.302				
2000	Kotochigova*et al.* [15]	3.306				
2000	Leo *et al.* [16]	3.321				
2000	Drag *et al.* [17]	3.137				
2002	Amiot and Dulieu [6]	3.295	1.296	5.744	3.07	
2003	Derevianko and Porsev [18]		1.38	6.01		
2010	Coxon and Hajigeorgiou [2]	3.31	1.2996	5.1363	2.677	1.87
2012	Hutson [19]	3.3209	1.3621			
2012	Mitroy [20]	3.2619	1.2955	5.3659	3.16338*	3.0407*

*sum of second- and fourth-order terms.

Table 2.2: Third-order dispersion coefficients C_m for the $X\,^1\Sigma_g^+$ and $a\,^3\Sigma_u^+$ states of Cs_2 in units of cm^{-1} $Å^m$.

Year	Author(s)	$10^{-11}C_{11}$	$10^{-13}C_{13}$
1985	Weickenmeier *et al.* [8]	-2.378	
1999	Patil and Tang [13]	-2.064	-2.677
2010	Coxon and Hajigeorgiou [2]	-2.378	-2.677
2012	Mitroy [20]	-2.1586492	-3.0032639

2.2 Direct-Potential-Fit Methods

A modern approach for analyzing diatomic molecular spectroscopic data is to perform a "direct potential fit" (DPF) to experimental data. This method compares experimental transition energies with eigenvalue differences calculated from a version of the one-dimensional Schrödinger equation [21]:

$$-\frac{\hbar^2}{2\mu}\frac{d^2\psi_{v,J}(r)}{dr^2} \; + \; [V(r) + V_{\rm C}(r)]\; \psi_{v,J}(r) = E_{v,J}\, \psi_{v,J}(r) \tag{2.5}$$

in which

$$V_{\rm C}(r) = \frac{J(J+1)\hbar^2}{2\mu r^2} \tag{2.6}$$

in which $\hbar$ is Planck's constant divided by 2π, μ is the reduced mass of the two atoms being considered, J is the rotational quantum number, $V(r)$ is the potential energy, $V_{\rm C}(r)$ is centrifugal potential, $E_{v,J}$ is the total energy, r is the internuclear distance and $\psi_{v,J}(r)$ is the unknown wavefunction to be solved for. The Schrödinger equation in Eq. (2.5) pertaining to a DPF is based on some parametrized potential energy function.

The rigid rotor description of diatomic molecules offers insight into the fundamental physical and mathematical problems associated with rotational and vibrational motion. In this approximation the rotations and vibrations are independent of one another. That is to say, the magnitude of the energies associated with a given rotation or vibration is not influenced by the other's motion. However, real molecules are not rigid and exhibit what is called centrifugal distortion. The vibrational energy level spacings are of larger magnitude than the rotational energy level spacings, so it is the magnitude of the rotational energy

level spacings that is affected by the vibrational motion of the molecule. The energy of a molecule in a given vibrational state υ can be described by a power series in $J(J+1)$:

$$E_{\upsilon,J} = G_\upsilon + B_\upsilon[J(J+1)] - D_\upsilon[J(J+1)]^2 + H_\upsilon[J(J+1)]^3 + L_\upsilon[J(J+1)]^4 + \cdots \quad (2.7)$$

By treating the centrifugal potential as a perturbation, the perturbed wavefunction can be determined as the solution of an inhomogeneous version of Eq. (2.5), centrifugal distortion constants $\{D_\upsilon, H_\upsilon, L_\upsilon, ...\}$ can be calculated for all vibrational levels for a particular potential [22]. With the advent of Hutson's technique [22], calculating the rotational constants for all levels of any given potential well became a routine procedure.

Using the energies from Eq. (2.7) as trial energies, an ansatz of the potential energy function can be obtained. The parameters defining the potential are then optimized by a non-linear least-squares fit. Effects due to atomic-mass-dependent adiabatic and non-adiabatic Born-Oppenheimer Breakdown (BOB) functions [21], and radial strength functions that account for splittings as a result of angular momentum coupling between electronic states [23, 24], are included in the appropriate effective radial Hamiltonian. This method was originally introduced for atom-diatom van der Waals molecules [25], but is now extensively used for diatomic molecule data analyses. For any spectroscopic transition, the energies of the lower and upper levels are eigenvalues of Eq. (2.5) for the appropriate potential energy function. Since Eq. (2.5) is an ordinary differential equation, it is solved by conventional methods, and the eigenvalue $E_{v,J}$ and eigenfunction $\psi_{v,J}$ may be readily determined for any specified vibration-rotation level $\{v, J\}$ of any given potential. The partial derivative of any eigenvalue with respect to any given potential function parameter can then be obtained from

the Hellman-Feynmann theorem [26]:

$$\frac{\partial E_{v,J}}{\partial p_j} = \left\langle \psi_{v,J}(r) \left| \frac{\partial V(r)}{\partial p_j} \right| \psi_{v,J}(r) \right\rangle \tag{2.8}$$

The differences between these partial derivatives for the upper and lower level of each observed transition are the partial derivatives of that transition energy with respect to the parameters $\{p_j\}$ required for the least squares fitting procedure.

Since a given data set usually consists of many transitions, an efficient algorithm for solving Eq. (2.5) is of tremendous value. In the present work, Eq. (2.5) is solved using the Numerov method, so a realistic trial energy for each vibration-rotational level in the system is of vital importance to the Schrödinger-solver subroutine. To address this problem, the subroutine must be supplemented with a procedure that identifies the highest vibrational level in the data set for each electronic state. Then, as the potential function parameters are optimized cyclically in the non-linear least squares fit, an automatic procedure will locate each pure vibrational level. An efficient way for performing this procedure is to use the semi-classical expression for the density of states [27]:

$$\frac{dv}{dG_v} = \frac{1}{2\pi}\sqrt{\frac{2\mu}{\hbar^2}} \int_{r_1(v)}^{r_2(v)} \frac{dr}{\sqrt{G_v - V(r)}} \tag{2.9}$$

The inverse of these derivatives provides a good approximation for distances between neighbouring vibrational levels. When the pure vibrational levels are known, Hutson's method can be employed to calculate the rotational band constants $\{B_v, D_v, H_v, L_v, ...\}$ appearing in Eq. (2.7). The fitting procedure considers each datum individually, and then uses the stored band constants to generate good trial eigenvalues for any desired $\{v, J\}$ state. Two

additional problems exist for using the DPF method: (i) choosing a flexible and physically sensible potential function form, and (ii) obtaining realistic trial potential function parameters for starting the fit. These are discussed in the following sections.

2.3 Potential Function Forms

Although the DPF method has been shown to be quite efficient for modeling simple single-well diatomic potential energy functions, the choice of the 'best' potential function form is still being contested [26]. The most popular potential forms have been: (i) polynomial potential forms, (ii) the Extended Morse Oscillator (EMO) potential form, (iii) the Morse/Long-Range (MLR) potential form, and (iv) the Spline-Pointwise Potential (SPP).

2.3.1 Polynomial Potential Functions

This type of potential function form is a simple polynomial expansion in some radial-coordinate. A polynomial potential function from early literature is the Dunham expansion [28]:

$$V(r) = a_0\xi^2(1 + a_1\xi + a_2\xi^2 + a_3\xi^3 + ...) \qquad \text{in which} \qquad \xi = \xi_{\rm Dun} = \frac{\rm r - r_e}{\rm r_e} \tag{2.10}$$

The fundamental problem with this potential form is that it always diverges outside the range of data used to determine it. In particular, $V_{\rm Dun}(r) \to +\infty$ or $-\infty$ as $r \to \infty$, which is clearly an unphysical property inherent in this type of function. To rectify this unphysical property of such expansions, Ogilvie proposed use of an alternative expansion variable that

approaches a finite limit when $r \to 0$ and $r \to \infty$ [29]:

$$\xi_{\mathrm{OT}}(r) = 2\left(\frac{r - r_{\mathrm{e}}}{r + r_{\mathrm{e}}}\right) \tag{2.11}$$

Although this variable does not diverge at very large or very small distances, polynomial functions of this variable can still behave nonphysically there [29].

It is possible to constrain such polynomial potential function forms such that they both incorporate the appropriate inverse-power long-range terms and approach the correct asymptotic limit [30]. However, to force such functions to incorporate such behaviour necessarily requires the use of much higher-order polynomials than would be required merely to represent the data. Introducing appropriate mathematical constraints into the potential function form may appear trivial [30], but the altered potential function has a tendency to oscillate above and below the dissociation limit in the long-range extrapolation region before eventually achieving the correct limiting behaviour. This kind of unphysical behaviour of simple expansions in the $\xi_{\mathrm{OT}}(r)$ variable suggests that a better radial variable and potential form should be sought after.

The divergent and/or oscillatory behaviour exhibited by simple power series expansion in ξ_{DUN} or ξ_{OT} are somewhat mitigated by using the radial variable introduced by Šurkus *et al.* [31]:

$$\xi^{(p)}_{\mathrm{Šur}}(r) = \frac{r^p - (r_{\mathrm{e}})^p}{r^p + (r_{\mathrm{e}})^p} \equiv y^{\mathrm{eq}}_p(r) \tag{2.12}$$

with $p > 1$. The Šurkus radial variable is confined to the range [-1,1] on the domain $[0, \infty)$. At large internuclear distances this variable can be expanded such that:

$$\xi_{\check{\mathrm{S}}\mathrm{ur}}^{(p)}(r) \simeq 1 - 2\left(\frac{r_\mathrm{e}}{r}\right)^p + \mathcal{O}\left(\frac{r_\mathrm{e}}{r}\right)^{2p} \tag{2.13}$$

Therefore, if $p = n$, where n is the power of the leading inverse-power term in the long-range potential, a potential function expressed as a power series in $\xi_{\check{\mathrm{S}}\mathrm{ur}}^{(p)}(r)$ may be constrained to have the theoretical value of the leading term from the long-range:

$$V(r) - \mathfrak{D}_\mathrm{e} \propto -C_p\left(\frac{r_\mathrm{e}}{r}\right)^p + \mathcal{O}\left(\frac{r_\mathrm{e}}{r}\right)^{2p} \tag{2.14}$$

where the constant C_p is defined in terms of the coefficients of the power series. The parameter p is often constrained to equal 6, because this leading van der Waals dispersion term is proportional to $1/r^6$. This leads the potential expressed as a simple power series in the Šurkus variable to lose its flexibility [32], since when p is large, the full range of $\xi_{\check{\mathrm{S}}\mathrm{ur}}^{(p)}(r)$ is attained on a smaller r domain. With such limited flexibility for large p, it also becomes impossible to model long-range limiting behaviour where there are several long-range inverse-power terms.

A practical way to avoid incorrect long-range potential behaviour is to attach a tail to the potential that forces it to exhibit the correct limiting long-range behaviour. This added component of the potential is a long-range inverse-power-sum of the form shown in Eq. (2.3) [10].

This is the approach used by a group at the University of Hanover in Germany [33]. They represented the potential energy function on a specified region between chosen inner r_- and outer r_+ turning points by a simple polynomial in the variable ξ_{Han}:

$$\xi_{\mathrm{Han}}(r) = \frac{r - r_m}{r + br_m} \tag{2.15}$$

where b is another fitted parameter. Although this modification includes the proper long-range limiting behaviour, the points of attachment r_- and r_+ are *ad hoc* choices and do not necessarily represent anything that is physically meaningful. Moreover, imposing smooth connections requires the assumption that polynomial potential function and its derivatives at the beginning and end of the selected data region are correct. This assumption may be questionable because the polynomial naturally exhibits unpredictable behaviour outside, and hence probably at the edges of, the data region. Therefore, this is an approach that one should avoid, if other options exist.

Ultimately, polynomial potential function forms have enough shortcomings that more sophisticated models became a necessity. In particular, fits to data that span a large fraction of the potential well typically require relatively high-order polynomials, and in fits to high-order polynomials, the coefficients are highly correlated, which makes convergence difficult to achieve. In practical work with polynomial potentials, these coefficients have often been reported to 18 significant digits, and using them would require quadruple precision arithmetic on most computers [33]. This attribute will obviously make the model less convenient for practical use. Moreover, since experimental transition energies are typically reported to only 8-10 significant digits, it seems unreasonable that numerous 18-digit polynomial coefficients be required to describe them.

2.3.2 Extended Morse Oscillator (EMO) Potential

Since polynomial potential function forms always behave nonphysically outside the experimental data region, theoreticians returned to the Morse potential. Replacing the constant coefficient in the exponential term by a polynomial in r, Coxon and Hajigeorgiou were able to devise a potential function form that not only fit experimental data accurately using a relatively modest number of expansion parameters, but could also provide a realistic description of the approach to the dissociation limit [34]. They called this function the "Generalized Morse Oscillator" (GMO), and it has the form:

$$V_{\mathrm{GMO}}(r) = \mathfrak{D}_{\mathrm{e}}(1 - e^{-\beta(r)\cdot(r-r_{\mathrm{e}})})^2 \tag{2.16}$$

in which $\beta = \beta(r)$ is a simple polynomial function centered at r_{e}. However, this potential form suffered from the same divergence problem as the Dunham potential did: *i.e.*, $\beta(r) \to \pm\infty$ as $r \to \infty$. Lee *et al.* [35] introduced the following potential which was later applied by Seto *et al.* [36]:

$$V_{\mathrm{EMO}}(r) = \mathfrak{D}_{\mathrm{e}}(1 - e^{-\beta(r)(r-r_{\mathrm{e}})})^2 \tag{2.17}$$

in which

$$\beta(r) = \beta_{\mathrm{EMO}}(r) = \sum_{\imath=0}^{N} \beta_i (y_p^{\mathrm{eq}}(r))^i \tag{2.18}$$

and

$$y^{\mathrm{eq}}(r) = y(r; r_{\mathrm{e}}) = \frac{r - r_{\mathrm{e}}}{r + r_{\mathrm{e}}} \tag{2.19}$$

Eq. (2.20) was later generalized to include powers of r and r_e greater than 1:

$$y_p^{eq}(r) = y_p(r; r_e) = \frac{r^p - (r_e)^p}{r^p + (r_e)^p} \tag{2.20}$$

Since the potential function is based around an exponential term, a small change in the exponent coefficient makes a large change in the function itself. Thus, for a given data intermolecular potential $\beta(r)$ is a relatively slowly varying function, and a relatively modest number of parameters can be used to represent it.

If the polynomial order in Eq. (2.18) is large, then Eq. (2.17) may still behave nonphysically on the interval between the data region and the lower and upper limits of y_p, -1 and +1, respectively. However, as the variable p increases, the opportunity for such behaviour is suppressed because of the nature of the functional mapping of $y_p(r)$ onto r [37, 24]. In particular, as p increases, the $y_p(r)$ values associated with the end points of the data region move closer to the endpoints of the domain of the expansion variable $y_p(r)$, +1 and -1 [24].

This potential function form has been used in a number of experimental data analyses [35, 37, 38]. It successfully reproduces the experimental data, yields accurate values of r_e, and yields realistic estimates of the well depth, when $\mathfrak{D}_e$ is a fitting parameter. The key feature of the Coxon and Hajigeorgiou innovation was that the potential well shape parameters would be controlled by a relatively slowly varying exponent coefficient function.

This modified version of this function created by Lee *et al.* is flexible, and can represent high-resolution data sets within experimental uncertainties; it extrapolates reasonably well outside the data region; it is continuous on $r \in \mathbb{R}$, and it can usually be defined by a modest number of variables. However, it does not have the correct long-range limiting behaviour. For the function to have the correct long-range limiting behaviour, the potential function

form needs to incorporate Eq. (2.3). However, reliable values for C_m coefficients are not always available, and if this is the case, the EMO model is perhaps the best potential energy function available for diatomic molecules.

2.3.3 Spline-Pointwise Potential (SPP)

The Spline-Pointwise Potential (SPP) is defined by a cubic spline function that passes through potential function values at a specified set of distances. The energies that define the individual points are varied during the DPF procedure. Tiemann and Wolf first used spline-pointwise potentials to model systems with shallow wells and quasi-bound levels [39, 40, 41, 42]. However, their original SPP methodology was quite capable of being unstable, and as such, had to be used with caution. Later Pashov *et al.* improved the SPP method by incorporating singular-value decomposition and proper partial derivatives into the least-squares procedure, and the resulting procedure was stable [43, 44, 45]. They also showed that the spline function could be written as a linear combination of basis functions associated with the N data points:

$$V_{\mathrm{SPP}}(r) = \sum_{i=1}^{N} V(r_i)\, S_i^N(r) \tag{2.21}$$

where $V(r_i)$ are the potential function values, r_i are the grid points in r, and $S_i^N(r)$ are parameter-independent functions that also serve to define the values of the partial derivatives with respect to the parameters $V(r_i)$ in the least-squares procedure.

The SPP function works well for fitting experimental data for single-minimum potentials [43, 44], and is as yet the only potential function form shown to be able to treat double-

minimum potentials [45]. This function does not, however, incorporate the correct theoretical long-range behaviour of Eq. (2.3) in any way. Moreover, this potential function form cannot extrapolate reliably outside the experimental data region, so its ability to make predictions is limited. As usually implemented, the spline function is constrained to have zero curvature at the endpoints of the spline region, and attaching a long-range term requires some *ad hoc* mathematics to achieve sensible attachment. This model cannot readily determine reliable estimates of C_m coefficients, since they are not explicit parameters of the model, nor can it provide accurate extrapolations to the dissociation limit. Additionally, even though physically interesting parameters such as r_e and $\mathfrak{D}_\mathrm{e}$ can be determined with this potential, they are not explicit parameters of the potential function itself.

2.3.4 Morse/Long-Range (MLR) Potential

The major shortcoming of the EMO potential is its inability to represent the true, theoretically known long-range behaviour of molecular interactions given by Eq. (2.3). It has been mentioned that if the EMO potential included Eq. (2.3), that it would then have the correct long-range limiting behaviour. The Morse/Long-Range potential (MLR) has essentially the same algebraic structure as the EMO, except that two modifications allow it to incorporate the correct limiting long-range behaviour. This new function has the form [32]:

$$V_\mathrm{MLR}(r) = \mathfrak{D}_\mathrm{e}\left[1 - \frac{u_\mathrm{LR}(r)}{u_\mathrm{LR}(r_\mathrm{e})} e^{-\beta(r)\cdot y_p^\mathrm{eq}}\right]^2 \tag{2.22}$$

in which $\mathfrak{D}_\mathrm{e}$ is the well-depth, r_e is the equilibrium internuclear distance, and u_LR is damped version of the inverse power sum of Eq. (2.3):

$$u_{\mathrm{LR}}(r) = \sum_{m_i}^{\mathrm{last}} D_{m_i}(r) \frac{C_{m_i}}{r^{m_i}} \tag{2.23}$$

The exponent coefficient function $\beta(r)$ is designed to force potential energy function to have the form of Eq. (2.3) when r becomes large. It has the form:

$$\beta(r) = y_p^{\mathrm{ref}}(r)\beta_\infty + [1 - y_p^{\mathrm{ref}}(r)] \sum_{i=0}^{N_\beta} \beta_i \, y_q^{\mathrm{ref}}(r)^i \tag{2.24}$$

in which

$$y_p^{\mathrm{ref}}(r) = y_p(r, r_{\mathrm{ref}}) = \frac{r^p - (r_{\mathrm{ref}})^p}{r^p + (r_{\mathrm{ref}})^p} \qquad , \qquad y_q^{\mathrm{ref}}(r) = y_q(r, r_{\mathrm{ref}}) = \frac{r^q - (r_{\mathrm{ref}})^q}{r^q + (r_{\mathrm{ref}})^q} \tag{2.25}$$

and r_{ref} is non-physical parameter such that $r_{\mathrm{e}} < r_{\mathrm{ref}}$.

When $r = r_{\mathrm{e}}$, $y_p^{\mathrm{eq}} = 0$ and $u_{\mathrm{LR}}(r) = u_{\mathrm{LR}}(r_{\mathrm{e}})$, and hence the potential energy function is at its minimum with a well depth of $\mathfrak{D}_{\mathrm{e}}$. This is a central feature of this potential function form. The coefficient $\beta(r)$ is normally represented as a constrained polynomial in the variables $y_p^{\mathrm{ref}}(r)$ and $y_q^{\mathrm{ref}}(r)$, and the nature of these variables means that it must approach a finite value as $r \to \infty$. The limiting value of this exponent β_∞ is then defined as:

$$\beta_\infty \equiv \lim_{r\to\infty} \{\beta(r)\, y_p^{\mathrm{eq}}(r)\} = \lim_{r\to\infty} \{\beta(r)\} = \ln\left(\frac{2\mathfrak{D}_{\mathrm{e}}}{u_{\mathrm{LR}}(r_{\mathrm{e}})}\right) \tag{2.26}$$

Since β_∞ represents the limit at long-range for the argument of the exponential, the

long-range limit of the MLR is:

$$\begin{aligned} V_{\rm MLR}(r) &\simeq \mathfrak{D}_{\rm e}\left[1-\frac{u_{\rm LR}(r)}{u_{\rm LR}(r_{\rm e})}e^{-\ln\left(\frac{2\mathfrak{D}_{\rm e}}{u_{\rm LR}(r_{\rm e})}\right)}\right]^2 \\ &\simeq \mathfrak{D}_{\rm e}-u_{\rm LR}+\mathcal{O}\left(\frac{{u_{\rm LR}}^2}{4\mathfrak{D}_{\rm e}}\right) \\ &\simeq \mathfrak{D}_{\rm e}-D_{m_1}\frac{C_{m_1}}{r^{m_1}}-D_{m_2}\frac{C_{m_2}}{r^{m_2}}-\cdots+\mathcal{O}\left(\frac{{u_{\rm LR}}^2}{4\mathfrak{D}_{\rm e}}\right)+\cdots \end{aligned} \tag{2.27}$$

Therefore, the MLR potential form incorporates the appropriate long-range behaviour.

Because the limiting long-range behaviour of the exponential term in the MLR is approximately equal to $1-A/r^p$, where A is a constant, the power p must satisfy the condition $p > m_n - m_1$, where $m_{\rm last}$ is the last long-range power in $u_{\rm LR}$ and m_1 is the power of its first long-range term [46]. For example, for diatomic molecular states that are formed from S-state atoms, the leading contributions to the long-range potential correspond to $m = \{6, 8, 10\}$, and to satisfy this condition, necessarily $p \geqslant 5$ [46, 32]. However, there is no analogous constraint on the value of q.

Both the EMO and MLR functions have their greatest strength in the fact that the empirical component governing the detailed shape of the function is contained within the argument of the exponential argument. This feature allows both models to describe sophisticated potential energy functions, with only a modest number of parameters. Both models explicitly depend on the equilibrium internuclear distance $r_{\rm e}$ and the well depth $\mathfrak{D}_{\rm e}$. However, only the MLR function effectively incorporates the correct, theoretically-known inverse-power long-range behaviour [10]. By its exponential form and incorporation of this correct long-range behaviour, this potential energy function requires many fewer parameters than do conventional polynomial potentials [46]. Arguably, the MLR form is the best potential energy function form yet devised for diatomic molecules. However, it has not yet

been shown to be capable of modeling potential energy functions that have abrupt changes in shape, such as a double minimum or a "shelf".

Damping Functions

The inverse-power sum used in the preceding section to represent the long-range potential energy curve of Cs_2 is known to diverge for all internuclear distances. That is to say, the simple inverse-power sum of Eq. (2.3), has singularities at both the short and long-range. Damping functions $D_m(r)$ that remove the singularities were introduced into the long-range potential energy function of the MLR in Eq. (2.22) [47]:

$$u_{\rm LR}(r) = \sum_{m=m_1}^{m_{\rm last}} D_m(r)\,\frac{C_m}{r^m} \tag{2.28}$$

Following the recommendation of Le Roy *et al.* [47], this work uses the $s = -1$ version of a generalized Douketis *et al.* type of damping function:

$$D_m^{{\rm DS}(-1)}(r) = \left(1 - \exp\left(-\frac{b^{\rm ds}(-1)(\rho r)}{m} - \frac{c^{\rm ds}(-1)(\rho r)^2}{m^{1/2}}\right)\right)^{m+s} \tag{2.29}$$

with ρ defined as:

$$\rho = \frac{2\rho_{\rm A}\rho_{\rm B}}{\rho_{\rm A} + \rho_{\rm B}} \tag{2.30}$$

in which $\rho_{\rm A}$ and $\rho_{\rm B}$ correspond to atom A and B, respectively, and $\rho_{\rm A}$ is defined as:

$$\rho_{\rm A} = \left(\frac{I_{\rm p}^{\rm A}}{I_{\rm p}^{\rm H}}\right)^{\frac{2}{3}} \tag{2.31}$$

where $I_{\mathrm{p}}^{\mathrm{A}}$ is the ionization potential of atom A and $I_{\mathrm{p}}^{\mathrm{H}}$ is the ionization potential of atomic hydrogen. For the cesium dimer the value ρ is 0.434. At very small r, $D_m(r)/r^m \propto r^{-1}$ and the quadratic term in the second line of Eq. (2.22) will dominate the potential energy function with a $1/r^2$ functional behaviour.

Theoretical C_1 coefficients

At very small internuclear distances, the potential curve of diatomic molecules is described coherently by the united atom (UA) approximation. The potential energy function has four physical contributions and can be approximated with [47]:

$$V_{\mathrm{UA}}(r) \backsimeq \frac{Z_{\mathrm{A}} Z_{\mathrm{B}} C_1^{\mathrm{pp}}}{r} + E_{\mathrm{AB}}^{\mathrm{el}}(r) - E_{\mathrm{A}}^{\mathrm{el}} - E_{\mathrm{B}}^{\mathrm{el}} \tag{2.32}$$

in which

$$C_1^{\mathrm{pp}} = \frac{e^2}{4\pi\epsilon_0} = 116149.97 \text{ cm}^{-1} \tag{2.33}$$

Z_{A} and Z_{B} are atomic numbers for atoms A and B, $E_{\mathrm{AB}}^{\mathrm{el}}(r)$ is the electronic energy of the united atom, and $E_{\mathrm{A}}^{\mathrm{el}}$ and $E_{\mathrm{B}}^{\mathrm{el}}$ are the total electronic energies of the individual atoms. The atomic number for the united atom is the sum of the atomic numbers of the individual atoms. The functional form of $V_{\mathrm{UA}}(r)$ dictates that the first contribution will become infinitely large as $r \to 0$. In the case of Cs_2, $Z_{\mathrm{A}} = Z_{\mathrm{B}} = 55$ so that the first contribution to $V_{\mathrm{UA}}(r)$ has a coefficient of $Z_{\mathrm{A}} Z_{\mathrm{B}} C_1^{\mathrm{pp}} = 3.5135366 \,\mathrm{x}\, 10^8$ cm^{-1}.

The very short-range behaviour of a diatomic potential energy function can be characterized using the first term of $V_{\mathrm{UA}}(r)$. On a plot of $V(r)$ vs. r, a linear equation with slope

$C_1^{\rm pp}$ is easily constructed by choosing two arbitrary values of r. A plot containing this linear function and a potential energy function on a logarithmic scale should exhibit one of two relationships. When $s = -1/2$ and as $r \to 0$, $V_{\rm MLR}(r) \propto 1/r$. Therefore, when $s = -1/2$ in the MLR damping function in Eq. (2.29), the potential energy curve should approach the same limiting behaviour as the first term in $V_{\rm UA}(r)$.

Fig. 2.1 displays the limiting short-range behaviour potential energy functions with increasing long-range complexity, as well as the theoretical coulombic behaviour. Potential energy functions for which $p = 1$ contain $u_{\rm LR}(r)$ functions that include only the leading term in the long-range function $u_{\rm LR}(r)$ of Eq. (2.23). Potentials that include the first two, three, four, five, and six terms in the long-range are labelled by p values of 3, 5, 6, 7, and 8, respectively. Table 2.3 lists the dispersion coefficients used to generate Fig. 2.1. The figure also includes a potential energy function for both states in which the value of s in the damping function is -1/2. All of the potential energy functions where $p \geq 5$ with $s = -1$ sho reasonable behaviour in the short-range region except the $p = 1$ potential for the triplet state.

Table 2.3: Dispersion coefficients used in the tests of the short-range behaviour for the $X\,^1\Sigma_g^+$ and $a\,^3\Sigma_u^+$ states of Cs_2.

Dispersion coefficient	Value
C_6 [19]	3.3207822×10^7 cm^{-1} Å^6
C_8 [19]	1.3621006×10^9 cm^{-1} Å^8
C_{10} [2]	5.1363×10^{10} cm^{-1} Å^{10}
C_{11} [2]	-2.378×10^{11} cm^{-1} Å^{11}
C_{12} [12]	2.68×10^{12} cm^{-1} Å^{12}
C_{13} [13]	-2.68×10^{13} cm^{-1} Å^{13}

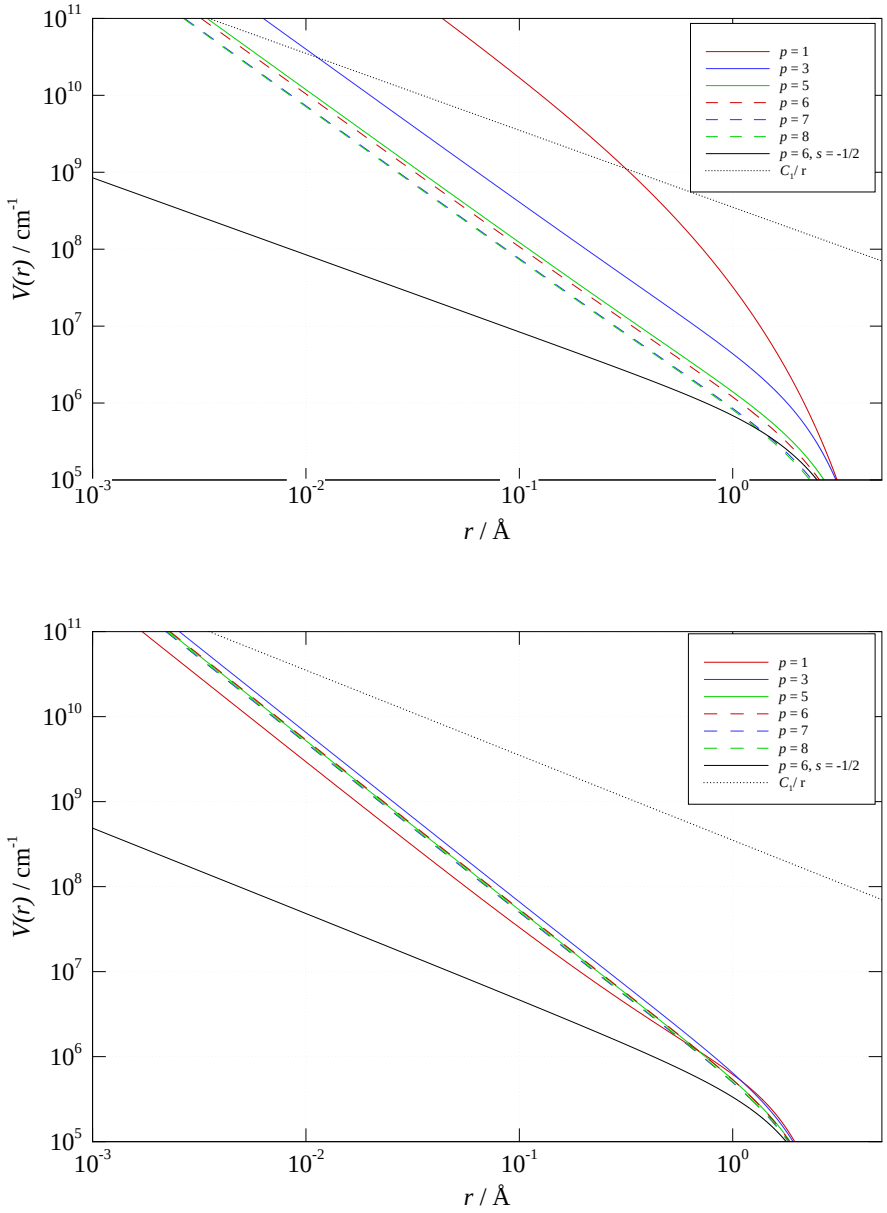

Figure 2.1: Plot of the short-range of various $q = 5$ potentials for the $X\,^1\Sigma_g^+$ (bottom) and the $a\,^3\Sigma_u^+$ (top) states of Cs_2.

2.4 Data for the $X\,^1\Sigma_g^+$ and $a\,^3\Sigma_u^+$ States of Cs_2

The first extensive high resolution observations of rovibrational transitions of the cesium dimer were obtained by Weickenmeier *et al.* utilizing optical double-resonance polarization spectroscopy [8]. In this study, transitions were observed involving levels up to $\upsilon = 140$, although vibrational energies are only reported up to $\upsilon = 137$. Approximately 2500 lines were observed from the transitions of the $C\,^1\Pi_u \leftarrow X\,^1\Sigma_g^+$ system including lines obtained from Raab *et al.* [48]. Weickenmeier's data set also included 400 Λ-type double-resonance signals from the $D\,^1\Pi_u^+ \leftarrow X\,^1\Sigma_g^+$ system [48], 80 V-type double-resonance signals from the $C\,^1\Pi_u \leftarrow X\,^1\Sigma_g^+$ system, and 450 fluorescence series lines [49]. The value determined for $\mathfrak{D}_\mathrm{e}$ was 3649.5 ± 0.8 cm^{-1}. Unfortunately, the original data set from this study is no longer available.

In 2002, Amiot and Dulieu determined a potential energy curve for the $X\,^1\Sigma_g^+$ state of Cs_2 using high-resolution laser-induced emission spectra, which comprises the core of the data used in the present analysis [6]. It consists of and includes 16 900 transitions from 113 main fluorescence series including observation of vibrational levels up to $\upsilon = 136$, which is bound by 24.1 cm^{-1}. However, only 16 668 transitions were made available for public use. It was determined that the most efficient way to obtain emission into the $X\,^1\Sigma_g^+$ state was to pump the first excited state, $A\,^1\Sigma_u^+$. Transitions in this data set have experimental uncertainties ranging from $0.001 - 0.003$ cm^{-1} with the majority having uncertainties of 0.001 cm^{-1}. Amiot and Dulieu determine an estimate of $\mathfrak{D}_\mathrm{e}$ 3649.88 ± 0.45 cm^{-1} by fitting Rydberg-Klein-Rees turning points to a version of Eq. (2.4) [27, 50, 51, 52], and they suggest that a reason for the large uncertainty is the influence of the hyperfine structure of Cs_2 which

broadens line widths up to 0.3 cm^{-1} at high v. Their data set also has multiple differing estimates for the energies of the highest vibrational levels, and they also mainly observed even values for J at these levels. In contrast, Weickenmeier *et al.* observed 4 series with odd J values and reported only one series with an even J value. Amiot and Dulieu argued that the observed difference in $\mathfrak{D}_e$ was due to the differences in estimates of the energies associated with the highest observed levels for even and odd values of J. In 2008, Danzl *al.* determined binding energies for v =73, 72, and 71 with uncertainties of 0.001 cm^{-1}, and estimated the dissociation for the $X\,^1\Sigma_g^+$ state very accurately [5].

In 2008, Xie *et al* observed the first 40 vibrational levels of the $a\,^3\Sigma_u^+$ state of Cs_2 [7]. Using perturbation facilitated infrared-infrared double resonance excitation into the $3\,^3\Pi_g$ state, resolved fluorescence into the $a\,^3\Sigma_u^+$ state was observed. The $a\,^3\Sigma_u^+$ and the $X\,^1\Sigma_g^+$ state approach the same asymptote as $r \to \infty$, and they exhibit hyper-fine splitting due to spin-orbit coupling effects. The very highest vibrational levels of the $X\,^1\Sigma_g^+$ and the $a\,^3\Sigma_u^+$ states of Cs_2 cannot be predicted using one-dimensional conventional models. Accurate determination of the highest vibrational levels of the respective states is of grave importance for obtaining potentials able to yield accurate scattering lengths.

Chin *et al.* observed more than 60 magnetic field-induced Feshbach resonances for both the $X\,^1\Sigma_g^+$ and $a\,^3\Sigma_u^+$ states of Cs_2 [4]. Coupled-states analyses of those resonances yielded the effective single-channel scattering length associated with the hyperfine-free limit for both states: 148.3 Å for the $X\,^1\Sigma_g^+$ state, and 1273 Å for the $a\,^3\Sigma_u^+$ state. The present work combines automated direct-potential fits to the above data sets with manual fits to these scattering lengths to obtain optimum effective potential energy functions for the $X\,^1\Sigma_g^+$ and $a\,^3\Sigma_u^+$ states of Cs_2.

With the data sets associated with the $X\,^1\Sigma_g^+$ and $a\,^3\Sigma_u^+$ states, along with the scattering lengths from coupled channel analyses, an optimal uncoupled channel potential for the two electronic states will be defined.

Chapter 3

Potential Parameter Determination

3.1 Optimization of the r_{ref} Parameter

The parameters that define the the MLR potential energy function each serve distinct purposes. The parameters $\mathfrak{D}_{\mathrm{e}}$ and r_{e} are of physical significance, and their values are accurately determined when an extensive and accurate data set is available for the potential fit. The quantity r_{ref} is non-physical parameter for which a rough preliminary value can be estimated from $r_{\mathrm{ref}} = \sqrt{r_- \cdot r_+}$, where r_- and r_+ are the inner- and outermost turning points of the highest observed vibrational level. While this geometric mean of the two turning points that define the highest observed vibrational level offer a reasonable ansatz for r_{ref}, it is not necessarily optimal.

A way of ascertaining the quality of a given potential energy function is by calculating the dimensionless root mean square (DRMS) deviation $\overline{dd}$:

$$\overline{dd} \equiv \left\{ \frac{1}{N} \sum_{i=1}^{N} \left[\frac{y_{calc}(i) - y_{obs}(i)}{u(i)} \right]^2 \right\}^{\frac{1}{2}} \tag{3.1}$$

in which $y_{calc}(i)$ is the calculated energy, $y_{obs}(i)$ is the observed energy, $u(i)$ is the uncertainty of the observed energy, and N is the number of experimental data. Minimization of the $\overline{dd}$ value implies an optimal direct-potential fit. In particular, it implies that the calculated energy values obtained from the molecular potential are very close to the observed energy values.

The parameters that have no physical significance offer an avenue for minimizing the value of $\overline{dd}$. To this end, r_{ref} is selected solely on it's ability to improve the quality of fit for the molecular potential. Given the form of the MLR potential energy function and curvature of the general shape of a diatomic potential energy curve, the other mathematical entity to consider is the polynomial in the exponent of the MLR defined in Eq. (2.24). The polynomial $\beta(r)$ is comprised of $N_\beta+2$ terms with $N_\beta+1$ free parameters, and these parameters allow the shape of a sophisticated potential energy function to be represented accurately. However, a potential energy function is considered compact when few parameters are needed to represent a potential curve, and compactness is desirable. The figures below capture the essence of parameter optimization as it applies to selecting polynomial-order and determining what r_{ref} value offers the minimal value of $\overline{dd}$ for a given polynomial-order. It is desirable to minimize the polynomial order, while the value of r_{ref} is seen to be arbitrary. Ideally, the order of the polynomial should offer a domain of stability for $\overline{dd}$ with respect to changes in the value of r_{ref}. Moreover, if a small change in r_{ref} leads to a large change in the value of $\overline{dd}$, then r_{ref} is not in a domain of stability. A domain of instability infers that the order of the polynomial should be increased until such a domain is found. Thus, minimizing $\overline{dd}$ is a problem that

spans two dimensions; the polynomial order and the value of $r_{\rm ref}$. The final consideration are the contributions of the parameters p and q in their respective radial expansion variables defined in Eq. (2.25). The minimum value p can have is determined by the the number of terms in Eq. (2.23). The value of p must be greater than the absolute difference of the powers of the first and last terms in Eq. (2.23). For example, if Eq. (2.23) includes C_6, C_8, and C_{10}, the absolute difference of the first and last terms is $|m_{\rm last} - m_1| = |10 - 6| = 4$, so $p \geq 5$. The chosen form of Eq. (2.23), and thus p, typically has little or no effect on $\overline{dd}$. The parameter q is not constrained to certain values; however, as q gets large, the range of $y_q^{\rm ref}$ is restricted to a narrower domain of r. As a result, choosing large value of q results in the potential energy function as a whole losing its ability to fit the data set as well as it could when a smaller value of q is selected.

Fig. 3.1-3.3 show how $\overline{dd}$ varies with $r_{\rm ref}$ for a number of families of potential energy functions, the associated with different polynomial orders and different values of p and q. Fig. 3.1 shows plots of $\overline{dd}$ as a function of $r_{\rm ref}$ when $\{p, q\} = \{5, 4\}$ and $\{p, q\} = \{5, 3\}$ for potential functions that include the first three terms of the long range. Fig. 3.2 shows results obtained for models with $\{p, q\} = \{6, 4\}$ and $\{p, q\} = \{6, 3\}$ that include the first four terms of the long range tail. Fig. 3.3 shows analogous plots for $\{p, q\} = \{7, 4\}$ and $\{p, q\} = \{7, 3\}$ potentials that include the first five terms of the long range. Table 3.1 lists the values of the dispersion coefficients used in the potentials used to generate Fig. 3.1-3.3.

In the bottom panel of Fig. 3.1, it can be seen that when $N = 11$ there is a very narrow domain of stability in $r_{\rm ref}$. Moreover, for a small change in $r_{\rm ref}$, there is a significant increase in $\overline{dd}$. For $N = 12$, the domain of stability is much larger than for $N = 11$, but its minimum does not correspond to the absolute minimum. When $N = 13$, a wide domain of stability

is obtained, as well as a minimum that matches the absolute minimum $\overline{dd}_{\min}$. There is no benefit to move from $N = 13$ to $N = 14$ thus, the chosen potential is $N = 13$ at the r_{ref} value that corresponds to the minimum. In the top panel of Fig. 3.1, it can be seen that when $N = 14$ the minimum of $\overline{dd}$ differs significantly from the minimum attained when $\{p, q\} = \{5, 4\}$. This significant decrease in fit quality from the bottom panel for $N = 14$ is due to the use of $q = 4$. For $N = 15$ and $N = 16$ domains of stability are obtained, but neither family of potentials reaches the absolute minimum that $N = 17$ reaches. Thus, $N = 17$ with $q = 4$ is the appropriate potential to choose at the r_{ref} value that corresponds to the absolute minimum.

In Fig. 3.2 and Fig. 3.3, similar trends are observed. In particular, both figures show that a larger polynomial order N is needed for both $p = 6$ and $p = 7$ when q is increased from 3 to 4. In Fig. 3.2, domains of stability and absolute minima are achieved with $N = 13$ and $N = 17$ for $q = 3$ and $q = 4$, respectively. In Fig. 3.3, domains of stability and absolute minima are achieved with $N = 13$ and $N = 17$ for $q = 3$ and $q = 4$, respectively. The long-range behaviours of the recommended models for each of the six potential energy function types considered in Fig. 3.1-3.3 are compared in Fig. 3.4.

Table 3.1: Dispersion coefficients used in the preliminary fits for the $X\,^1\Sigma_g^+$ of Cs_2 [2].

Dispersion coefficient	Value
C_6	$3.31\,\mathrm{x}\,10^7$ cm^{-1} Å^6
C_8	$1.2996\,\mathrm{x}\,10^9$ cm^{-1} Å^8
C_{10}	$5.1363\,\mathrm{x}\,10^{10}$ cm^{-1} Å^{10}
C_{11}	$-2.378\,\mathrm{x}\,10^{11}$ cm^{-1} Å^{11}
C_{12}	$2.677\,\mathrm{x}\,10^{12}$ cm^{-1} Å^{12}

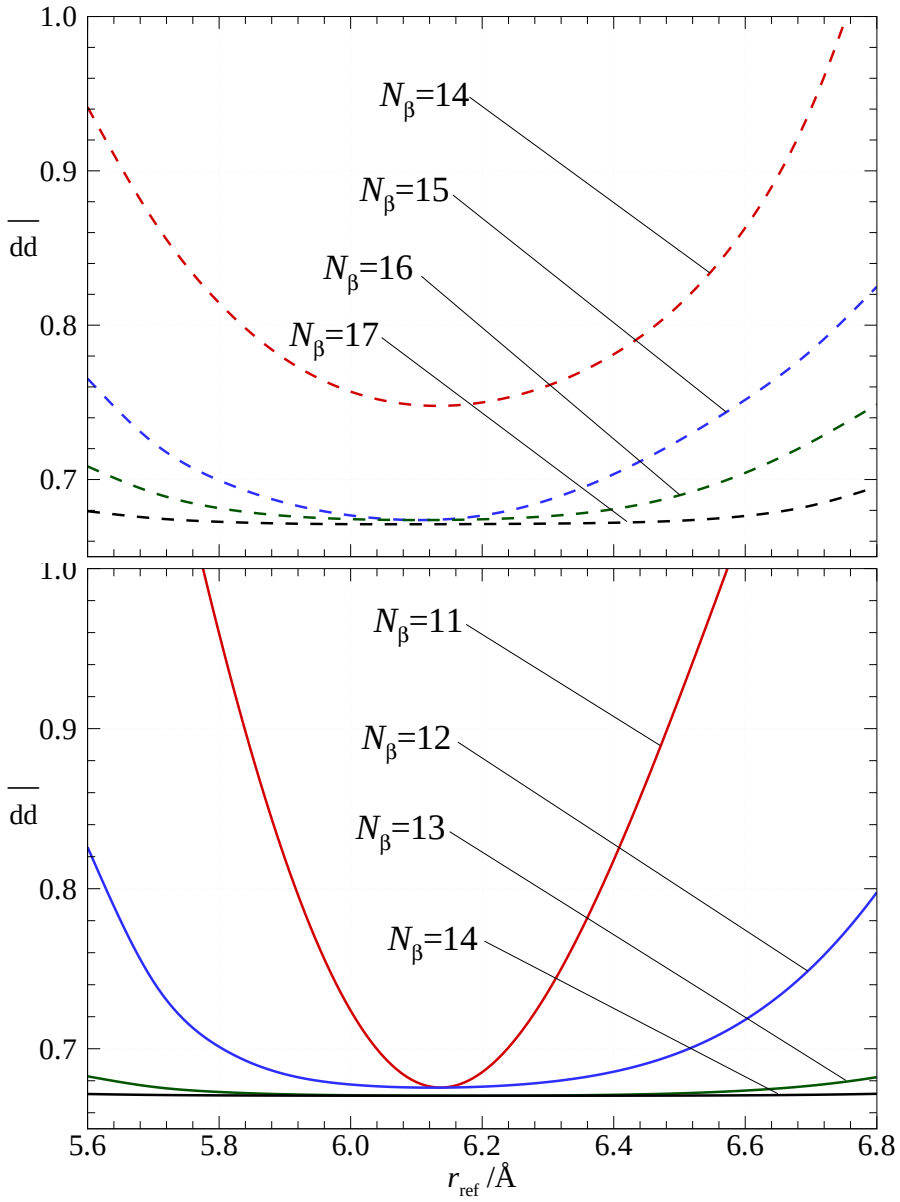

Figure 3.1: Plot of $\overline{dd}$ as a function of r_{ref} for MLR function models with three inverse power terms in $u_{\text{LR}}(r)$ ($m = 6, 8$, and 10) and $\{p, q\} = \{5, 4\}$ (top) and $\{p, q\} = \{5, 3\}$ (bottom).

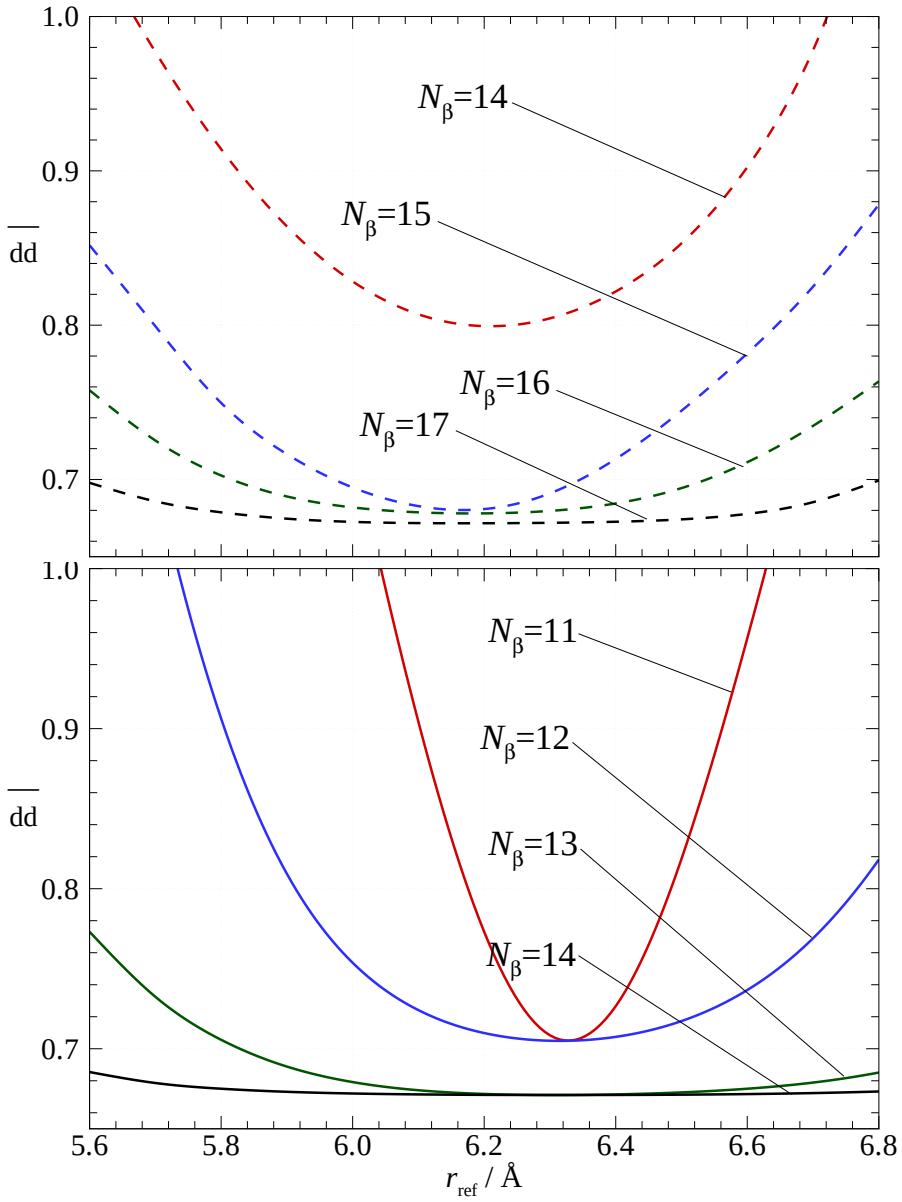

Figure 3.2: Plot of $\overline{dd}$ as a function of r_{ref} for MLR function models with four inverse power terms in $u_{\text{LR}}(r)$ ($m = 6, 8, 10$, and 11) and $\{p, q\} = \{6, 4\}$ (top) and $\{p, q\} = \{6, 3\}$ (bottom).

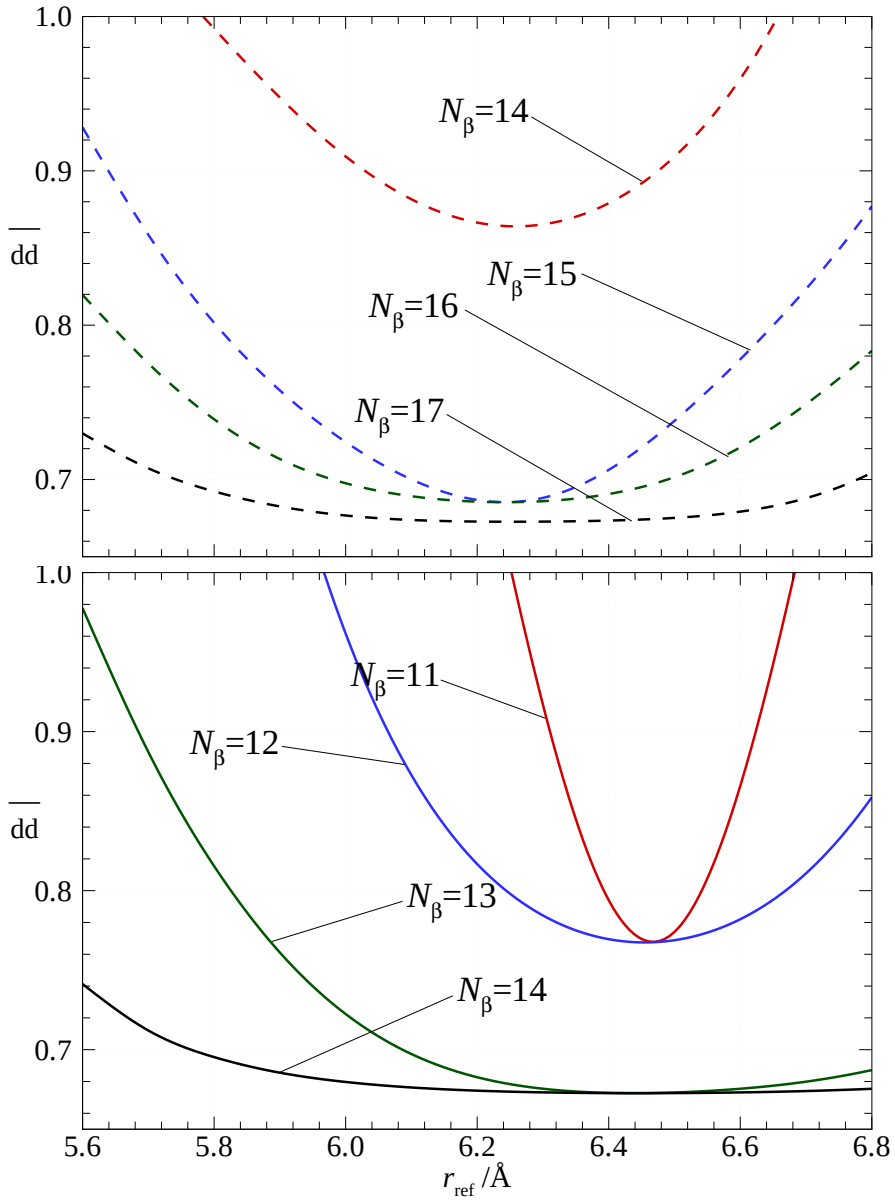

Figure 3.3: Plot of $\overline{dd}$ as a function of r_{ref} for MLR function models with five inverse power terms in $u_{\text{LR}}(r)$ ($m = 6, 8, 10, 11,$ and 12) and $\{p, q\} = \{7, 4\}$ (top) and $\{p, q\} = \{7, 3\}$ (bottom).

3.2 The Long-Range Tail of Diatomic Potentials and Scattering Lengths

3.2.1 Analysis of the Extrapolation Region

In order to examine the extrapolation behaviour of a molecular potential on the interval between the end of the data region and the asymptotic limit, it is useful to examine the behaviour of the function defined in terms of the fitted potential $V(r)$ and the leading long-range coefficients C_m. The fundamental requirement for rearranging Eq. (2.27) to isolate a particular C_m coefficient is that the coefficient actually be present in the potential energy function model. We can rearrange Eq. (2.27) to obtain an effective C_6 coefficient, which we denote by $C_6^{\rm eff}(r)$ which would define the full interaction potential if it was written as $V(r) = \mathfrak{D}_{\rm e} - C_6(r)/r^6$:

$$C_6^{\rm eff}(r) \;\equiv\; r^6[\mathfrak{D}_{\rm e} - V(r)] \;\simeq\; C_6 \;+\; \frac{C_8}{r^2} \;+\; \frac{C_{10}}{r^4} \;\ldots \tag{3.2}$$

Similarly, $C_8^{\rm eff}(r)$ would characterize the deviation of the full potential from the limiting $V(r) = \mathfrak{D}_{\rm e} - C_6/r^6$ behaviour, and at long-range it should take on the form:

$$C_8^{\rm eff}(r) \quad\equiv\quad r^8 \left[\, \mathfrak{D}_{\rm e} \; - V(r) - \; \frac{C_6}{r^6} \,\right] \;\simeq\; C_8 \;+\; \frac{C_{10}}{r^2} + \; \frac{C_{11}}{r^3} \;\ldots \tag{3.3}$$

Similarly for C_{10} and C_{11}:

$$C_{10}^{\rm eff}(r) \equiv r^{10}\left[\mathfrak{D}_{\rm e} - V(r) - \frac{C_6}{r^6} - \frac{C_8}{r^8}\right] \simeq C_{10} + \frac{C_{11}}{r} + \ldots \quad (3.4)$$

$$C_{11}^{\rm eff}(r) \equiv r^{11}\left[\mathfrak{D}_{\rm e} - V(r) - \frac{C_6}{r^6} - \frac{C_8}{r^8} - \frac{C_{10}}{r^{10}}\right] \simeq C_{11} + \frac{C_{12}}{r} + \ldots \quad (3.5)$$

From the form of the functions of $C_6^{\rm eff}(r)$, $C_8^{\rm eff}(r)$, and $C_{11}^{\rm eff}(r)$, when $C_6^{\rm eff}(r)$ and $C_8^{\rm eff}(r)$ are plotted against $1/r^2$ and $C_{11}^{\rm eff}(r)$ is plotted against $1/r$, the limiting slopes are C_8, C_{10} and C_{12}, respectively. Thus, as $r \to \infty$ the functions $C_6^{\rm eff}$, $C_8^{\rm eff}$, and C_{11}, should exhibit a positive slope in the limit when $r \to \infty$. The curvature of these functions should be positive or negative, depending on the sign of the second succeeding term. For example, the curvature of $C_6^{\rm eff}$ versus $1/r^2$ should be positive, as the second term to succeed it in the extrapolation region is a positive C_{10}. Similarly, the limiting curvature of $C_8^{\rm eff}$ versus $1/r^2$ should be negative or positive, depending on whether the C_{11} or C_{12} term is dominant. Conversely, the function $C_{10}^{\rm eff}$ versus $1/r$ should exhibit a negative slope of C_{11}. Using $C_m^{\rm eff}$ plots we are able to test whether or not our potential behaves correctly in the extrapolation region.

Preliminary work on Cs_2 used potential energy functions with various $u_{\rm LR}$ forms. In particular, the first potential energy functions developed to fit to the $X\,^1\Sigma_g^+$ and $a\,^3\Sigma_u^+$ states of Cs_2 used $u_{\rm LR}$ functions that were comprised of the first three, four and five dispersion coefficients known from theory. MLR potentials that have $u_{\rm LR}$ functions that are comprised of the first γ dispersion coefficients from Eq. (2.4) will be denoted as "MγLR" or "MγLR$_{p,q}^{\rm ref}(N_\beta)$". The $C_6^{\rm eff}(r)$ plots shown in the lower panel of Fig. 3.4 show that all of the potentials consid-

ered here display the correct limiting slope and curvature inside the extrapolation region. Each potential approaches a limit of C_6 as $r \rightarrow \infty$, while simultaneously approaching a slope of C_8. The curvature is also positive which is consistent with a positive C_{10} being the next leading term in u_{LR}. Our model form predicts that curvature should be negative or positive, respectively, on M4LR and M5LR plots for $1/r^2 < 0.008$ $\mathrm{\AA}^{-2}$. The $C_8^{\mathrm{eff}}(r)$ plots in Fig. 3.4 depict a variation of curvature with a change in the form of the potential energy function. Differences in curvature begin well before the extrapolation region begins and an increase divergence is more dramatic for certain potential energy functions. Each potential shown contains a C_{10} in its u_{LR}, but all but one function exhibits an inflection point. While these potentials approach the correct asymptotic limit, and delineation from theoretically predicted curvature necessitates choosing a different potential model. Moreover, our M3LR, M4LR, and M5LR models need $q > 4$ to impose initial negative curvature.

In principle, all of the curves in the $C_8^{\mathrm{eff}}(r)$ plots in Fig. 3.4 should approach an intercept of of C_8 with a limiting slope of C_{10} and weak negative curvature due to the small negative C_{11} value. However, for most of these potentials, the plots deviate drastically from the predicted limiting slope, which shows that they are unreliable models for the true potential. Ultimately, the recommended model is $\mathrm{M5LR}_{7,5}^{5,7}(18)$.

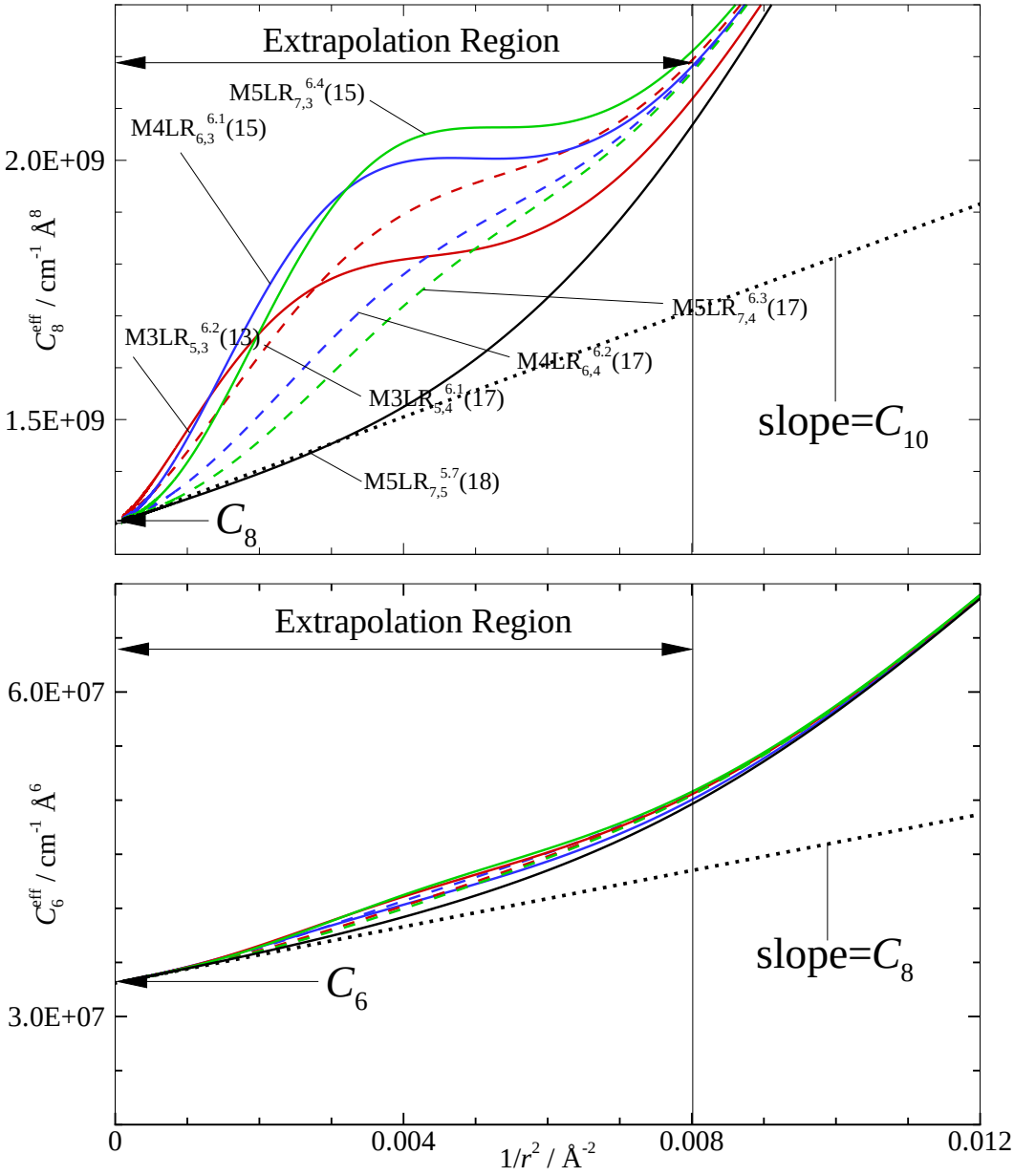

Figure 3.4: Plot of $C_6^{\text{eff}}(r)$ and $C_8^{\text{eff}}(r)$ as a function of $1/r^2$ for the $X\,^1\Sigma_g^+$ state of Cs_2 for the seven fitted potentials labelled in the C_8^{eff} panel.

3.2.2 The C_6 Dispersion Coefficient as a Variable

Collisional properties are of fundamental importance to the study of ultra cold Cs_2. The collisional cross section of a gas comprised of atoms approaches $\sigma = 4\pi a_s^2$ as $E \to 0$, where a_s is the s-wave scattering length [1]. From scattering theory we get the formal definition of the scattering length:

$$a_s = \lim_{k \to 0} \frac{1}{k} \cot\left[\eta_s(k)\right] \tag{3.6}$$

in which η_s is the s-wave scattering phase shift at collision wavenumber $k = \sqrt{2\mu E/\hbar^2}$ where $\mu = M/2$ for identical atoms of mass M.

As $r \to \infty$, the wavefunction for a given vibrational level dies off exponentially. Fig. 3.5 shows that when $E \to \mathfrak{D}_e$, $E - V(r)$ in the Schrödinger equation goes to zero, so:

$$\psi''(r) = \frac{2\mu}{\hbar^2} \left[E - V(r)\right] \psi(r) \ \to 0 \tag{3.7}$$

and the wavefunction curvature, goes to zero. Thus, the limiting behaviour of the wavefunction is a linear function, a tangent line. This wavefunction is of particular significance for a quantum mechanical understanding of the scattering length of a given electronic state. If the limiting slope of the wavefunction at zero collision energy has a tangent line drawn to it, there is a fixed point in which the tangent line for $\psi(r)$ will go to zero. The internuclear distance corresponding to the fixed point where the tangent line goes to zero is equal to the s-wave scattering length. If the limiting slope of the wavefunction at the dissociation limit is 0, then the line will be parallel to the axis and the scattering length will be of infinite magnitude. This concept can be developed further by invoking semi-classical theory which shows

that $a_s \propto 1/\sqrt{E_{\upsilon_{\max}}}$ [53], in which $E_{\upsilon_{\max}}$ is the binding energy of the highest vibrational level of the molecular potential. When $E_{\upsilon \max} \to 0$, the highest vibrational is coincident with the dissociation limit. Furthermore, $a_s \to \infty$ as $E_{\upsilon_{\max}} \to 0$.

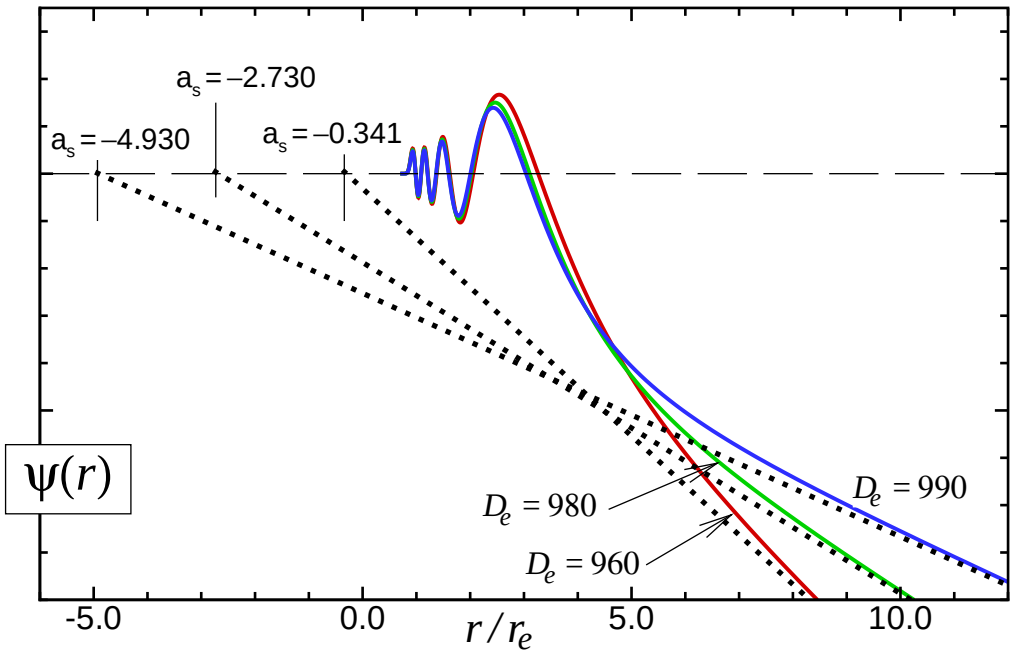

Figure 3.5: Plot of wavefunctions $\Psi(r)$ at collision energy $E = 0$ for Lennard-Jones (12,6) potentials as functions of r/r_e with a range of different well-depths in cm^{-1}, and their associated scattering lengths [1].

Fig. 3.5 shows that a_s becomes increasingly negative as the capacity of the potential to support vibrational levels increases. By extrapolation, it is clear that after $a_s \to -\infty$, increasing well-capacity further will give a_s a very large positive value (in the limit $+\infty$), and as a_s decreases from $+\infty$, the potential well will support another bound level. Thus, as well capacity systematically increases or decreases, a_s will pass through a succession of singularities as additional vibrational levels are added to or removed from the system. Just as varying well-capacity by changing $\mathfrak{D}_e$ can add vibrational levels, increasing C_6 will increase well-capacity and add vibrational levels.

In the case of the $X\,^1\Sigma_g^+$ of Cs_2, the value of the well-depth is largely fixed by the photoassociation data for v =73, 72, and 71, so the net well-capacity may only be modified by changing well-width at energies above those levels, and in practice this may be done by varying one or more of the C_m long-range coefficients. Since the fluorescence series data of Amiot and Dulieu [6] allows the vibrational levels within the data region to be determined quite accurately, changing the potential in this region would cause an undesirable increase in the value of $\overline{dd}$. Therefore, it is most desirable to change the potential in the extrapolation region, as it will have a smaller effect on the overall $\overline{dd}$ value of the potential. Chapter 2 outlines the various literature values that exist for the dispersion coefficients of Cs_2. It also outlines the disagreement in the scientific community regarding what are the true values of these various coefficients. Given the variation in the literature and its overall contribution to u_{LR}, it is sensible to assume that a small change in C_6 will create a significant change to the position of the highest vibrational levels, and thus, change the scattering length. Increasing the magnitude of the term $-C_6/r^6$ causes the potential to become deeper on the outer potential wall as C_6 becomes larger. As the potential wall is moved further from the vertical

axis with increasing C_6, the highest vibrational level moves further from the asymptotic limit. If the value of C_6 is increased yet further, the molecular potential adds a vibrational level whose wavefunction has one more loop (and node) than for the level that was previously the last $v_{\max}$. Assuming a small change in C_6 has a small affect on $\overline{dd}$, modifying C_6 in this analysis will force the potential to have a scattering length that matches the value of Chin *et al.* work [4].

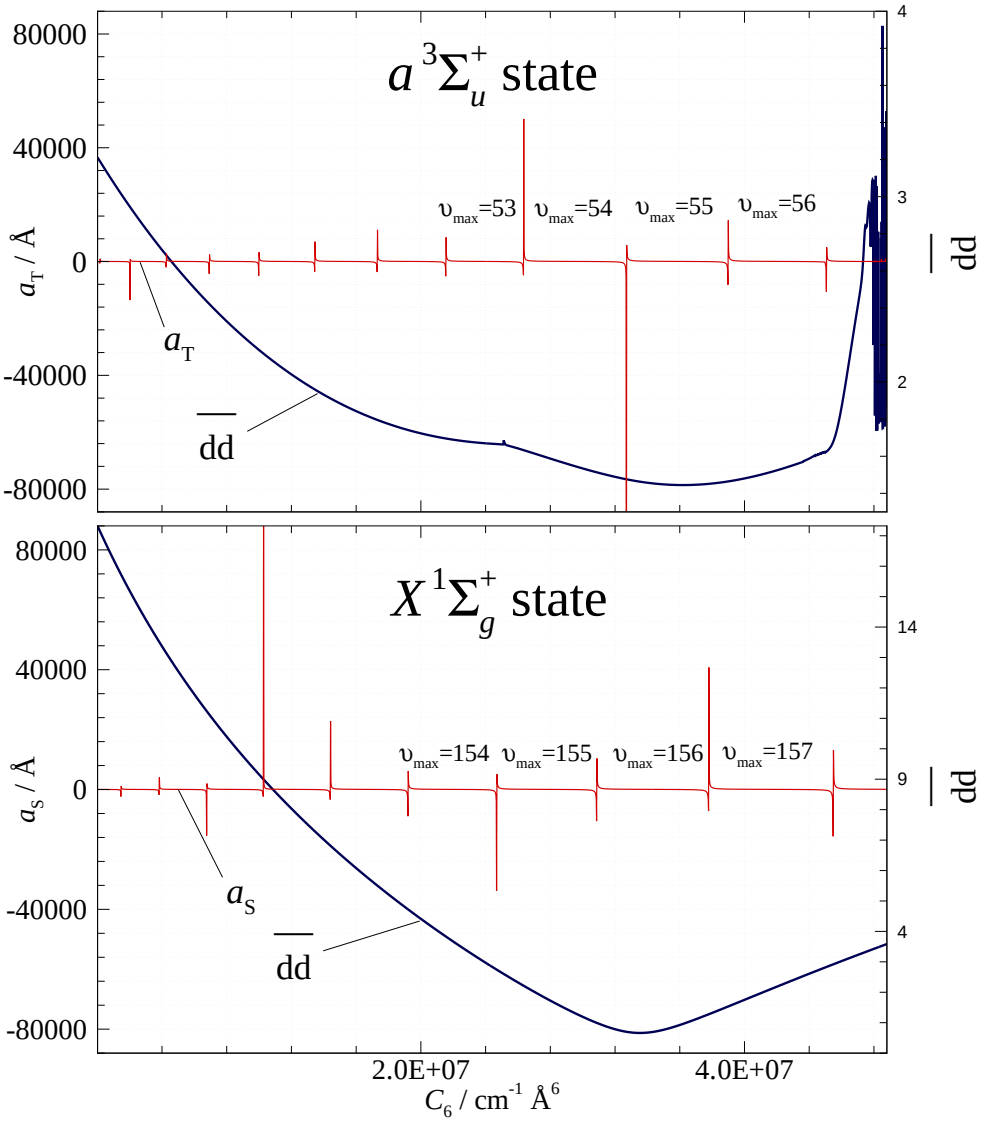

Figure 3.6: Plot of the scattering length and $\overline{dd}$ as a function of C_6 for the $X\,^1\Sigma_g^+$ (bottom) and the $a\,^3\Sigma_u^+$ (top) states of Cs_2 with M5LR$^{5.7}_{7,5}$(18) and M5LR$^{7.2}_{7,5}$(3), respectively.

Fig. 3.6 is constructed from the results of 5000 potential fits, 2500 for each electronic state. The dispersion coefficients in the long-range of these potential fits are held fixed, however, for each distinct potential fit, a different value of C_6 is chosen. The domain of the x-axis is [20000,50000000] with a mesh size of 20000. Fig. 3.6 shows the influence that C_6 has on the scattering lengths and the $\overline{dd}$ values for associated fits to spectroscopic data of the $X\,^1\Sigma_g^+$ and the $a\,^3\Sigma_u^+$ states of Cs_2. Sharp spikes in the scattering length plots show that as the highest vibrational level moves further from asymptotic limit, the scattering length goes to $-\infty$ with increasing C_6. The $\upsilon_{\max}$ values indicate the highest vibrational level of the potential between adjacent singularities.

Figure 3.7 is a companion to Fig. 3.6 which shows how the number of vibrational levels, and hence the $\upsilon_{\max}$ values vary with C_6 for both potentials. Each "step", or unit increase in $\upsilon_{\max}$ in Fig. 3.7 corresponds to a "spike" or singularity in Fig. 3.6. There is evidently a point where $\overline{dd}$ reaches a minimum value and it lies near a singularity for both states. However, Fig. 3.7 shows instability for the fitted $X\,^1\Sigma_g^+$ state potentials when $C_6 < \ 2.4\,\mathrm{x}\,10^7$ cm^{-1} Å due to the unphysical addition of vibrational levels. The absence of spikes in the a_{S} plot Fig. 3.6 is due to the high density of singularities and the scale of the x-axis. Fig. 3.9 shows that $X\,^1\Sigma_g^+$ state potentials, where $C_6 < \ 2.4\,\mathrm{x}\,10^7$ cm^{-1} Å, have additional potential minima. The potentials in Fig. 3.6 exhibit far more singularities than can be visibly discerned on the chosen mesh size. This result infers that the width of a potential can only decrease so much before the potential has to change drastically to accommodate the u_{LR} function. These potentials where $C_6 < \ 2.4\,\mathrm{x}\,10^7$ cm^{-1} Å^6 accommodate this drastic decrease of C_6 by adding potential minima. Fig. 3.8, confirms the hypothesis that the unphysical nature of the potentials with $C_6 < \ 2.4\,\mathrm{x}\,10^7$ cm^{-1} Å^6 for the $X\,^1\Sigma_g^+$ state of Cs_2 is due to the presence

of photoassociation spectroscopy data in the potential fit. The unphysical nature and low quality of fit suggests that the $X\,^1\Sigma_g^+$ state of Cs_2 should have minimal change of C_6 to obtain the desired scattering length. Ideally then, the decision to decrease or increase C_6 should be determined by which change offers the best minimization of $\overline{dd}$.

At the end of the C_6 domain in Fig. 3.6, the triplet state exhibits convoluted structure on its $\overline{dd}$ plot. The few fitted potentials that actually converge near the end of the domain have $\overline{dd}$ values that essentially oscillate from one fitted potential to the next. Moreover, the first fitted potential at $C_6 < \ 4.8\,\mathrm{x}\,10^7$ cm^{-1} Å has a $\overline{dd}$ value that is much greater than the $\overline{dd}$ value that precedes it.

Changing the value of C_6 to force the $X\,^1\Sigma_g^+$ state of Cs_2 to yield the correct experimental scattering length has one obvious implication. The value of C_6 chosen for the $X\,^1\Sigma_g^+$ is not necessarily going to be the ideal C_6 to give the correct scattering length for the $a\,^3\Sigma_u^+$ state of Cs_2. Thus, a different procedure is necessary to force the $a\,^3\Sigma_u^+$ state of Cs_2 to have the correct scattering length if C_6 is to be used to yield the correct scattering length for the $X\,^1\Sigma_g^+$ state. Section 3.3.3 discusses how the r_{ref} parameter from Eq. (2.25) can be varied to alter the well-capacity of the $a\,^3\Sigma_u^+$ state potential and thus, the scattering length. Moreover, Section 3.3.3 will discuss why the r_{ref} parameter cannot be used to yield the desired scattering length for the $X\,^1\Sigma_g^+$ state of Cs_2.

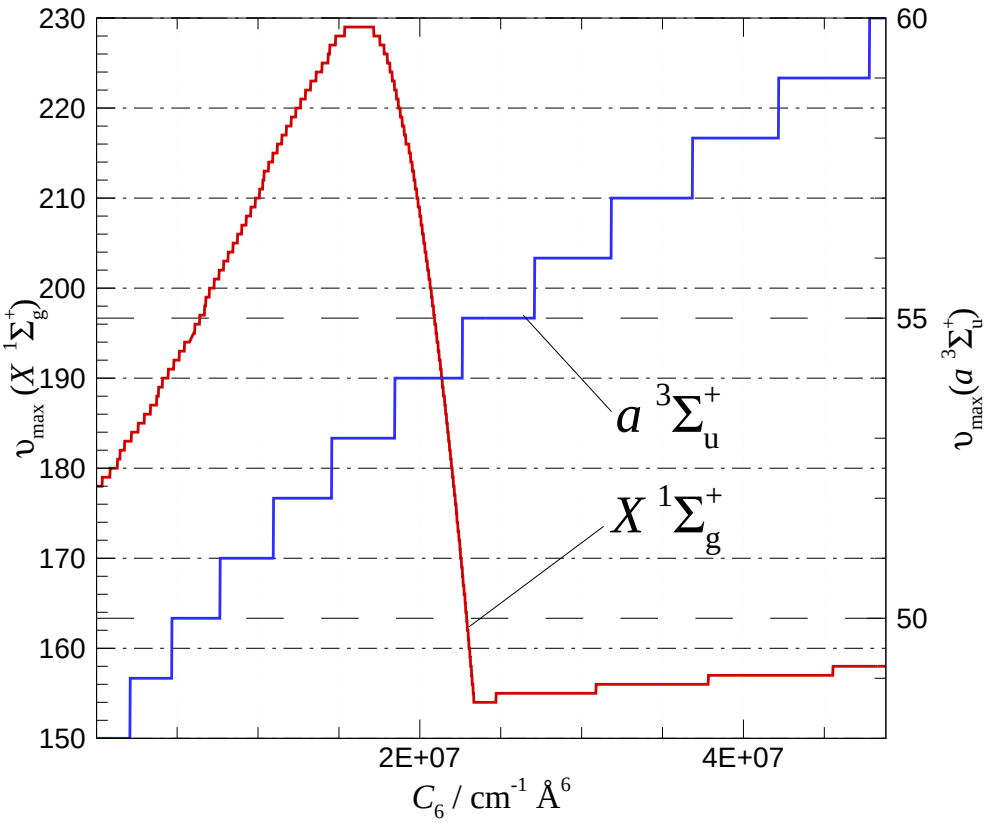

Figure 3.7: Plot of $\upsilon_{\max}$ as a function of C_6 for the $X\,^1\Sigma_g^+$ (right vertical axis) and the $a\,^3\Sigma_u^+$ (left vertical axis) states of Cs_2 for the same potential models considered in Fig. 3.6.

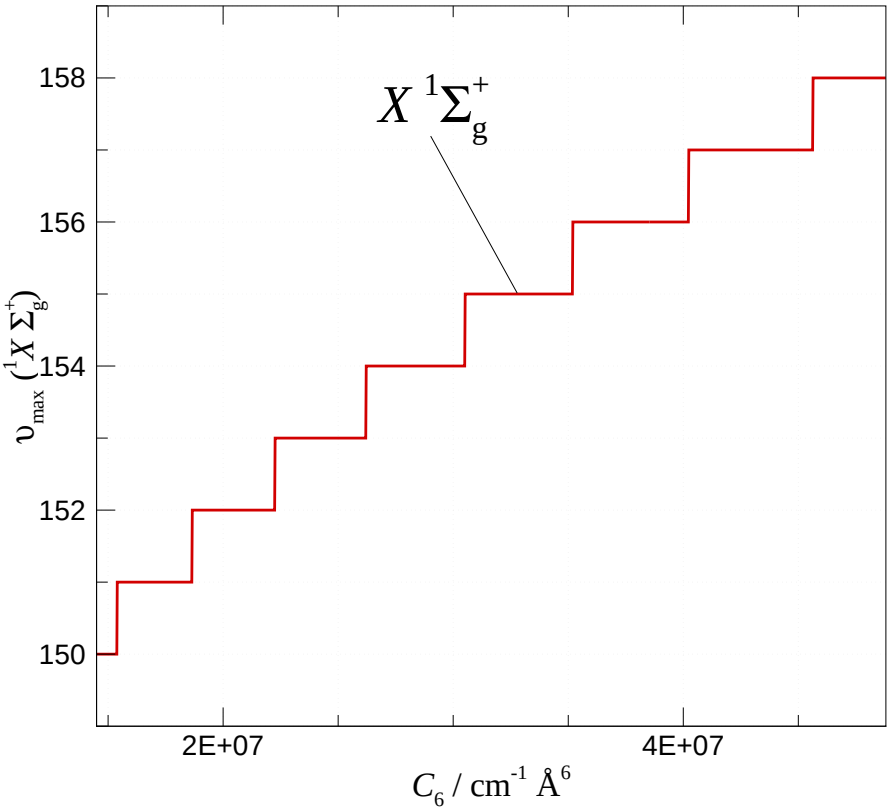

Figure 3.8: Plot of $\upsilon_{\max}$ as a function of C_6 for potentials obtained for the $X\,^1\Sigma_g^+$ state of Cs_2 with the photoassociation spectroscopy data omitted.

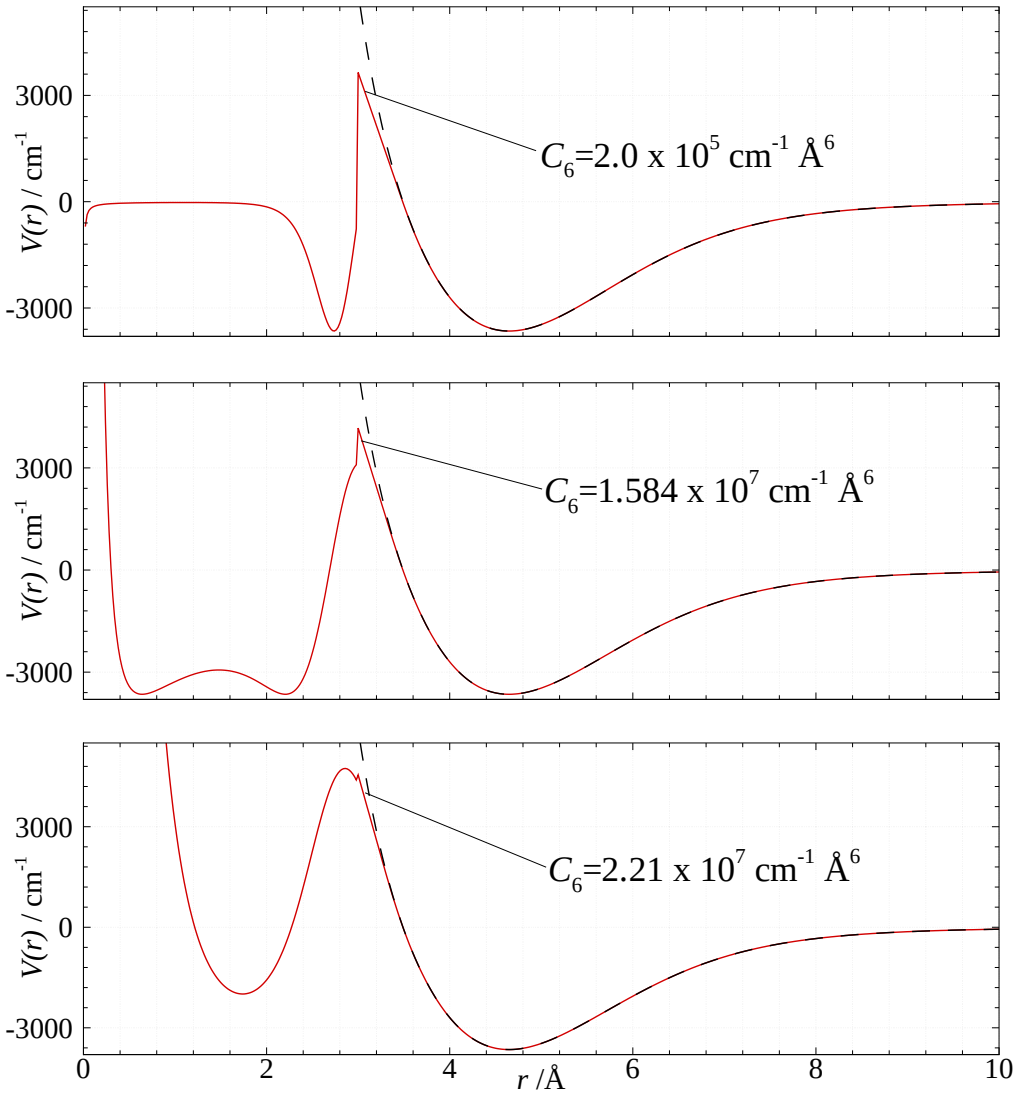

Figure 3.9: Plot of selected $X\,^1\Sigma_g^+$ state potentials with different C_6 coefficients. The black curve corresponds to $C_6 = 3.118\,\mathrm{x}\,10^7$.

3.2.3 Fitting to Scattering Lengths with $r_{\rm ref}$

The preceding section discussed the obvious problem that exists with altering the value of C_6 while minimizing $\overline{dd}$. In particular, if the value of C_6 is used to obtain the correct scattering length for one molecular state, it cannot then be altered for the second state if both states are to have identical long-range tails. Since the other non-physical parameters p, q, and C_6 are constrained for reasons already discussed, the only parameter that can be used to alter the scattering length of the other electronic state is $r_{\rm ref}$. Fortunately, Fig. 3.10 shows that changing $r_{\rm ref}$ can alter the scattering length in a way similar to the way C_6 does. However, most scattering length singularities on this $r_{\rm ref}$ plot do not display the full tangent function shape because the $r_{\rm ref}$ mesh size was too large. The scattering length becomes increasingly negative as $r_{\rm ref}$ increases, and approaches a singularity as another bound level is admitted to the well. This shows that for this case, increasing $r_{\rm ref}$ increases well capacity.

An analogous plot to Fig. 3.10 for the $X\,^1\Sigma_g^+$ state of Cs_2 in Fig. 3.11 shows instability as $r_{\rm ref}$ is increased. In particular, as $r_{\rm ref}$ is varied for the singlet state, an optimal value of $\overline{dd}$ exists on a small domain of $r_{\rm ref}$. In addition to this confined domain of stability, the optimal value of $\overline{dd}$ is not coincident with the singularity. When N_β is odd, as it is in Fig. 3.10, it exhibits behaviour similar to that in Fig. 3.6, but when N_β is even, the value of the scattering length increases as it approaches a singularity and it loses a vibrational level with increasing $r_{\rm ref}$ after passing through the singularity. While the physical implications of the $r_{\rm ref}$ parameter are not understood completely, the scattering length for an MLR potential always increases with $r_{\rm ref}$ when N_β is even, and always decreases when N_β is odd. This trend in the scattering length occurs for both the $X\,^1\Sigma_g^+$ and $a\,^3\Sigma_u^+$ state of Cs_2. This is

of great consequence as it implies that the way in which r_{ref} affects well-capacity can be controlled. In particular, for odd values of N_β, increasing r_{ref} increases well capacity as shown by the addition of vibrational level, and for even values of N_β, decreasing r_{ref} then decreases well-capacity as seen in Fig. 5.1.

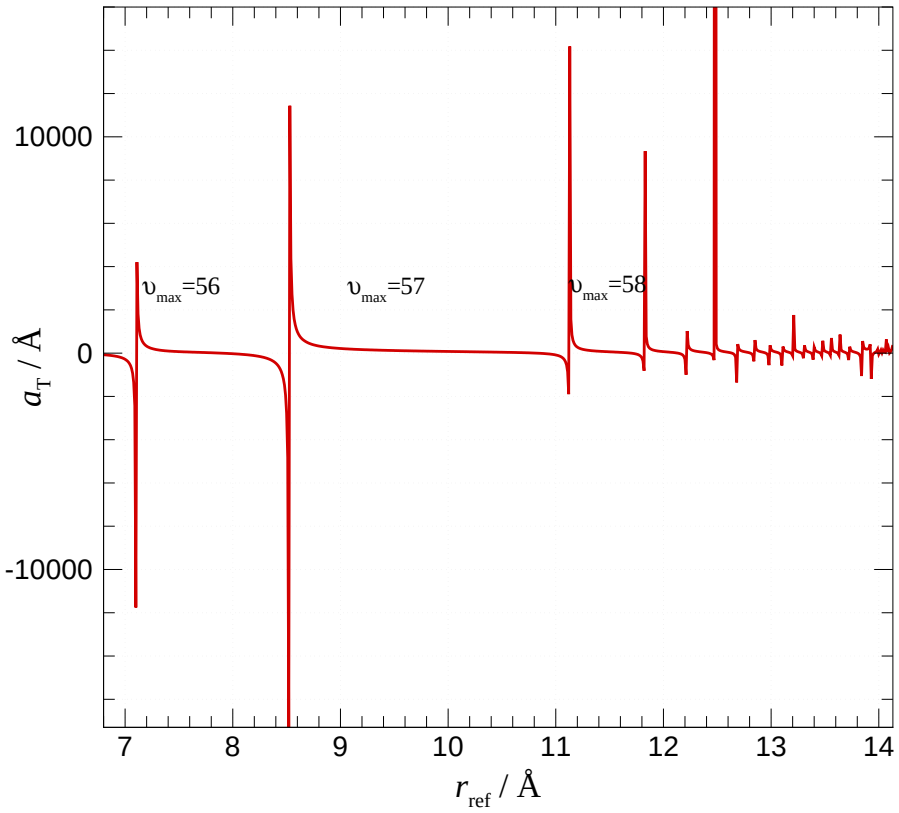

Figure 3.10: Plot of the scattering length for the $a\,^3\Sigma_u^+$ state of Cs_2 as function of r_{ref} with $\mathrm{M5LR}_{7,5}^{r_{\mathrm{ref}}}(3)$ and $C_6 = 3.31\,\mathrm{x}\,10^7$.

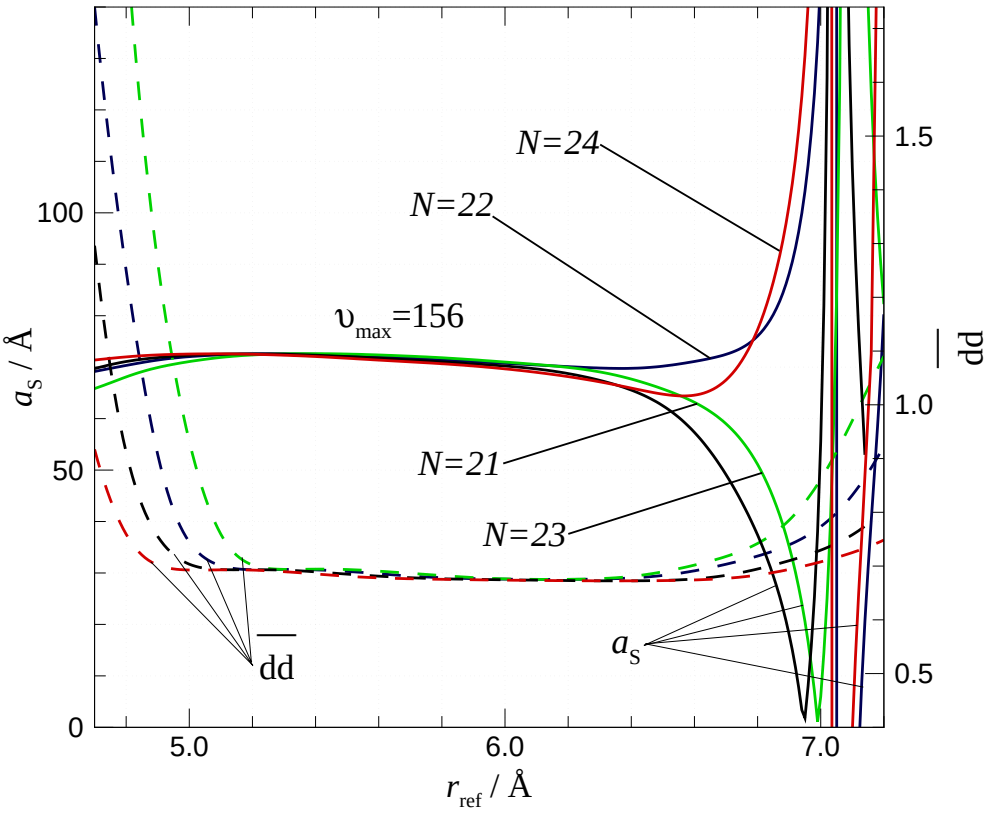

Figure 3.11: Plot of the scattering length for the $X\,^1\Sigma_g^+$ state of Cs_2 as function of r_{ref} for $N_\beta = \{21, 22, 23, 24\}$ with $\mathrm{M5LR}_{7,5}^{r_{\mathrm{ref}}}(N_\beta)$ and $C_6 = 3.320782\,\mathrm{x}\,10^7$.

3.3 Exchange Interaction Energy

Experimental determination of fluorescence series transitions for Cs_2 has not exceeded $\upsilon = 140$. Moreover, experimental data of Weickenmeier *et al.* [8] is not available, so levels above $\upsilon = 136$ can not be used in direct potential fits [2]. Work by Vanhaecke *et al.* sought to characterize high lying levels of $X\,^1\Sigma_g^+$ and $a\,^3\Sigma_u^+$ utilizing a coupled channel asymptotic approach using "nodal lines" to define the inner turning points. The short-range behaviour of the levels of both potentials was defined by a "nodal wall" located near 7.9 Å , and allowed for an analysis that considered exclusively the vibrational levels where spin-orbit coupling is observed. Their potential in this region has the form:

$$V(r) = -\sum_{n=6,8,10,12} \frac{f_n(r)\,C_n}{r^n} + (-1+2S)D\,r^\gamma\,e^{-2\alpha r} \tag{3.8}$$

in which the exponential "exchange" term is attractive for the $X\,^1\Sigma_g^+$ state, $S = 0$, and repulsive for the $a\,^3\Sigma_u^+$ state, $S = 1$, while the inverse-power terms are all attractive with identical coefficients for both electronic states. Here $V(r)$ is in units of wavenumbers (cm^{-1}). The damping coefficients $f_n(r)$ are given by:

$$f_n(r) = \left[1 - e^{-a(r-nb)}\right]^n \tag{3.9}$$

Vanhaecke et al. were not interested in determining absolute quantum numbers for the vibrational levels that they observed, and as a result the potential needed to be recreated to definitively define the vibrational levels. Table 3.2 lists the values of the parameters used to recreate this asymptotic potential energy for Cs_2. Our calculated vibrational levels for this potential are in Table 3.3, and are denoted with negative quantum numbers. For example,

for $v = -1$, this vibrational level is the last bound level, but an absolute assignment label for the quantum numbers cannot be made. The single positive vibrational level denoted by an asterisk lies above the asymptotic limit. The fact that Vanhaecke et al. used this model led to the consideration of of incorporating their exchange energy function in the long-range tail of the MLR used in this analysis.

Table 3.2: Parameters defining the dispersion-exchange potential of Vanhaecke *et al.* [3] for the $X\,^1\Sigma_g^+$ and $a\,^3\Sigma_u^+$ states of Cs_2.

Parameter	Value
C_6	3.299429048893501x10^7 cm^{-1} Å^6
C_8	1.2996298086453866x10^9 cm^{-1} Å^8
C_{10}	5.1363361927233055x10^{10} cm^{-1} Å^{10}
C_{12}	3.0700512808022114x10^{12} cm^{-1} Å^{12}
D	8214.469945 cm^{-1} Å$^{-\gamma}$
a	0.91286 Å^{-1}
b	0.37595 Å
α	1.011003481
γ	5.542

Table 3.3: Calculated vibrational levels for the $X\,^1\Sigma_g^+$ state of Cs_2 using the Vanhaecke *et al.* "nodal wall" potential.

v	G_v	v	G_v	v	G_v
-35	-274.46038	-23	-46.21481	-11	-3.98210
-34	-229.89394	-22	-39.40567	-10	-2.95808
-33	-196.75091	-21	-33.42666	-9	-2.13576
-32	-169.93282	-20	-28.19118	-8	-1.48852
-31	-147.41986	-19	-23.62220	-7	-0.99188
-30	-128.13636	-18	-19.65055	-6	-0.62321
-29	-111.41648	-17	-16.21376	-5	-0.36142
-28	-96.80764	-16	-13.25509	-4	-0.18674
-27	-83.98172	-15	-10.72294	-3	-0.08054
-26	-72.68913	-14	-8.57035	-2	-0.02514
-25	-62.73285	-13	-6.75462	-1	-0.00368
-24	-53.95262	-12	-5.23695		

However, incorporating the theoretical exchange function into Eq. (2.23) proved to be impossible because it caused $u_{\rm LR}(r_{\rm e})$ to be negative for the $a\,^3\Sigma_u^+$ state. This in turn causes β_∞ to be undefined thus, destroying the most fundamental component of the MLR potential energy function.

In the case of Cs_2, exchange energy can qualitatively be interpreted as an energy function that governs the onset of the difference between the $X\,^1\Sigma_g^+$ and $a\,^3\Sigma_u^+$ states. In particular, the exchange energy $V_{\rm EX}(r)$ can be defined as:

$$V_{\rm EX}(r) \equiv \frac{V_{\rm T}(r) - V_{\rm S}(r)}{2} = D\, r^{\gamma}\, e^{-2\alpha r} \tag{3.10}$$

in which $V_{\rm T}(r)$ is the potential energy of the $a\,^3\Sigma_u^+$ state and $V_{\rm S}(r)$ is the potential energy of the $X\,^1\Sigma_g^+$ state. In an attempt to see whether this potential energy contribution was implicitly included in the overall fitted potentials for both states, a series of fits to the data were performed for both states in which otherwise identical models with increasingly sophisticated $u_{\rm LR}(r)$ functions were used for the long-range tails of the two states. Table 2.3 presents the dispersion coefficients used for these models.

In Fig. 3.12, the theoretical exchange, the right-hand side of Eq. (3.10), is represented by the solid black curve. Fig. 3.12 depicts that for increasingly complex MγLR potentials, or for each additional long-range coefficient included in Eq. (2.23), the theoretical exchange is included when $\gamma > 2$. Moreover, MLR potentials that include the first three leading terms in Eq. (2.3) adhere to behaviour predicted by the theoretical exchange.

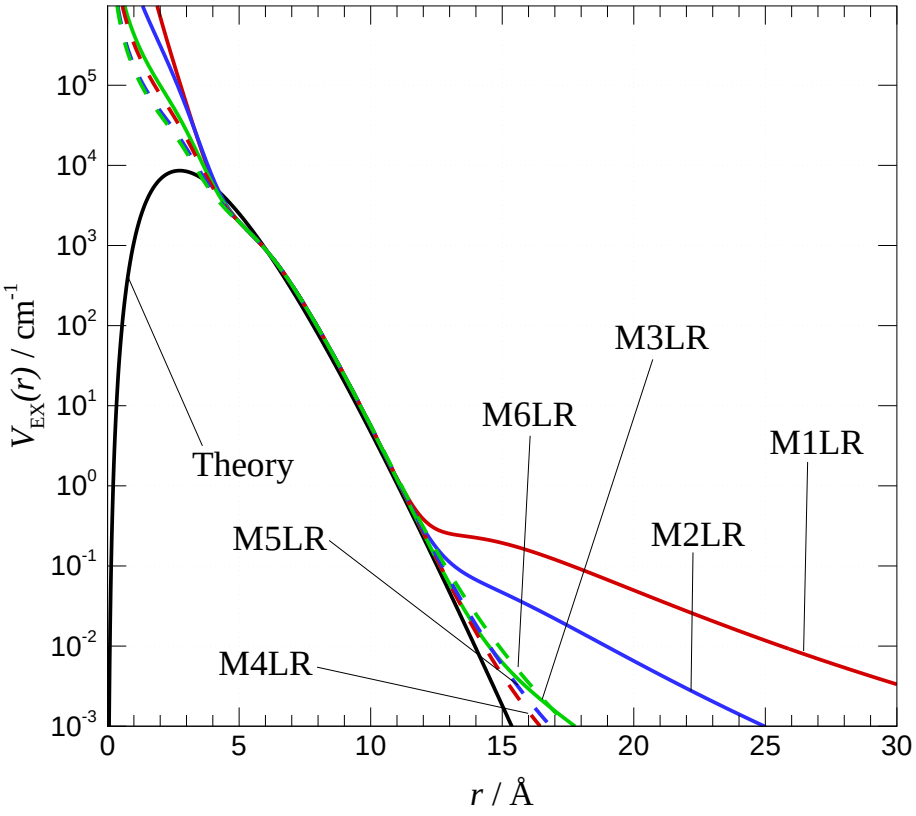

Figure 3.12: Plot of the exchange interaction energy derived from MLR potential fits and a theoretical exchange function.

Chapter 4

The $X\,^1\Sigma_g^+$ State of the Cesium Dimer

4.1 Previous Work on the $X\,^1\Sigma_g^+$ State of Cs_2

The most recent detailed study of the $X\,^1\Sigma_g^+$ state of the Cs_2 dimer was the DPF analysis by Coxon and Hajigeorgiou reported in 2010 [2]. The data set that they used was a collection of 16 544 fluorescence series line positions associated with the $A^1\Sigma_u^+ \rightarrow X^1\Sigma_g^+$ electronic transition. Their study used a modified version of the MLR in which two new parameters are introduced:

$$V_{\mathrm{MLR3}}(r) = \mathfrak{D}_{\mathrm{e}}\left(1 - \frac{u_{\mathrm{LR}}(r)}{u_{\mathrm{LR}}(r_{\mathrm{e}})}e^{-\beta_{\mathrm{MLR3}}(r)\,y_{p,a}(r,r_{\mathrm{e}})}\right)^2 \tag{4.1}$$

where

$$\beta_{\mathrm{MLR3}} = [1 - y_{r,m}(r, r_{\mathrm{ref}})]\sum_{i=0}^{N_\beta}\beta_i[y_q(r; r_{\mathrm{ref}})]^i + y_m(r; r_{\mathrm{ref}})\beta(\infty) \tag{4.2}$$

and

$$y_{p,a}^{\rm eq}(r, r_{\rm e}) = \left(\frac{r^p - {r_{\rm e}}^p}{r^p + a{r_{\rm e}}^p} \right) \tag{4.3}$$

This model differs from that of Eq. (2.22) in that the integer parameter p of Eq. (2.25) is replaced by two parameters, m and p, and by the introduction of the parameter a in the denominator of the right hand side of Eq. (4.3). Coxon and Hajigeorgiou's best fit used an 18-order polynomial with $\{p, m, q\} = \{5, 6, 4\}$, $r_{\rm ref}$=5.47 Å and $a = 1.79$, and this model generated a reported $\overline{dd} = 0.6063$. However, they did not present any results to justify a need for the new parameters m and a.

In Coxon and Hajigeorgiou's work, they report removing 122 lines from the original data set. They also fit their potential to data up to $\upsilon = 135$ rather than $\upsilon = 136$, thus removing 2 additional lines. It has proved to be impossible to determine which lines were removed, so it was necessary to generate Coxon and Hajigeorgiou's potential and run a fit to the same data set used for the potential fits in this work. Moreover, the reproduction of Coxon's potential used the complete data set rather than a modified data set that removed 124 transitions. This potential was generated by modifying the code to the program DPotFit to include the extra parameters m and a. The result of this fit was a potential with $\overline{dd} = 0.670679$. Subsequently, this potential had its long-range tail analyzed by utilizing $C_m^{\rm eff}$ plots.

4.2 Fitting Results and Analysis

The fluorescence series transitions reported by Amiot and Dulieu [6] naturally guide a fitted MLR potential energy function to approach the $F_a + F_b = 3 + 3$ limit of Danzl *et al.* which is reported as 3649.6874 cm^{-1} [5]. The two energy spacings that separate the 3+3 and 4+4

limits from the 3+4 limit are spaced equally by 0.3066332 cm^{-1}. Each atom has a total spin degeneracy of $2F + 1$, thus atoms with $F = 3$ and $F = 4$ have degeneracies of 7 and 9, respectively. Therefore, the hyperfine limits $F_a + F_b = 3 + 3,\ 3 + 4$, and $4 + 4$ have total degeneracies of $(7)(7) = 49$, $(7)(9) = 63$, and $(9)(9) = 81$. If the 3+3 limit is taken as the zero of energy, the energy difference between the 3+3 limit and the hyperfine-free limit is given by:

$$\begin{aligned} \frac{[63 + (2)(81)] \cdot [0.3066332\ \text{cm}^{-1}]}{49 + 63 + 81} &= 0.357473806\ \text{cm}^{-1} \\ &\approx 0.3575\ \text{cm}^{-1} \end{aligned}$$

This gives a predicted hyperfine-free dissociation limit of 3649.6874 cm^{-1} + 0.3575 cm^{-1} = 3650.0449 cm^{-1}. The spacing from the 3+3 limit to the hyperfine-free limit is used to adjust the three binding energies for $v = 73,\ 72$, and 71 reported by Danzl *et al.* [5]. With the addition of this energy spacing to these three binding energies, a DPF using the MLR will be constrained to extrapolate to the hyperfine-free limit.

Section 3.3.2 describes how the limiting slope of the wavefunction influences the magnitude of the scattering length. Moreover, due to the influence the long-range function u_{LR} has on the curvature of the continuum wavefunction at the dissociation limit, the parameters that define the potential energy function can be varied until the desired wavefunction is acquired. It is most logical to vary the leading term in u_{LR} as it has the largest contribution to the long-range of the potential energy function. As discussed earlier, for the $X\,^1\Sigma_g^+$ and $a\,^3\Sigma_u^+$ states of Cs_2 the leading dispersion coefficient is C_6.

The fitted potential presented in this section has parameters that were chosen based on the selection methods presented Chapter 3. In particular, the value of p was selected based on the first and last terms in $u_{\rm LR}(r)$, the value of q was selected based on the results from Fig. 3.4, and $r_{\rm ref}$ and N_β were selected based on their ability to minimize the value of $\overline{dd}$. Fig. 4.1 plots the scattering length $a_{\rm S}$ as a function of C_6 for the $X\,^1\Sigma_g^+$ state. This figure was constructed with 100 different $\mathrm{M3LR}_{5,5}^{6,2}(22)$ potentials, each optimized with respect to all other parameters while fixing the value of C_6. The other parameters used as input for the potential fit were identical for each potential fit. However, when the fit is complete, and the best potential fit is found for the parameters that are held fixed, the parameters that are allowed to vary change to optimize the quality of fit *i.e.* $\mathfrak{D}_{\rm e}$, $r_{\rm e}$, and the set of β_i. The functionality of $a_{\rm S}$ exhibits cotangent-like behaviour as a function of the leading dispersion coefficient C_6. As C_6 increases, so does the attractive force of the overall $u_{\rm LR}$ function. In particular, the potential well capacity increases and the binding energy of level $\upsilon_{\rm max}$ decreases. The singular behaviour of the cotangent function is exhibited, and $a_{\rm S}$ becomes increasingly negative. When the scattering length reaches $+\infty$, the molecular potential gains a vibrational level *i.e.* $\upsilon_{\rm max}$ increases by 1. In Fig. 4.1, only one singularity is visible, however, Fig. 3.6 shows that on the domain of $0 < C_6 < 4\,\mathrm{x}\,10^7$ other singularities were observed. The importance of observing additional singularities is the insight it provides into what is an appropriate value C_6. Between adjacent singularities $a_{\rm S}$ becomes small and passes through a value of 0. If the $u_{\rm LR}$ function represents the true long-range behaviour of a particular molecular potential, then it must impart the true scattering length.

The components of the $u_{\rm LR}(r)$ function in this analysis are a C_6, C_8, and C_{10}. Initially, the values used for each coefficient came from studies completed by Derevianko *et al.* [14, 18]

that employ a rigourous technique using electronic structure theory, and there has been no study since theirs that offers improved values. Their C_6 coefficient from 1999 is equal to $3.302\,\mathrm{x}\,10^{-8}$ cm^{-1} Å^7 [14], and is of similar magnitude to other values in the literature. Their C_8 and C_{10} coefficients from 2003 are equal to $1.38\,\mathrm{x}\,10^9$ cm^{-1} Å^8 and $6.01\,\mathrm{x}\,10^{10}$ cm^{-1} Å^{10}, respectively [18]. By varying the value of C_6 on the domain of [30000000,40000000], the singularity corresponding to an analytical potential with an infinite scattering length is located. With an appropriate mesh size of C_6, one can see both the curvature of the singularity and "find" the desired scattering length. Figure 4.1 illustrates how the scattering length becomes increasingly negative as C_6 is increased from 30000000 cm^{-1} Å^6 to larger values. At approximately 32600000 cm^{-1} Å^6, a singularity is observed where the potential has a scattering length of infinite magnitude and $E_{\upsilon_{\max}} = \mathfrak{D}_\mathrm{e}$. As C_6 is increased beyond its singular value, the scattering length has large positive values. After sufficiently increasing the value of C_6 beyond the singularity, an analytical potential with the desired scattering length is determined. The final C_6 obtained from Fig. 4.1 is $3.3164\,\mathrm{x}\,10^7$ cm^{-1} Å^6, and is reported in table 4.1.

Section 3.3.1 outlined the procedure by which the behaviour of a potential in the extrapolation region is analyzed. It was also shown that models using $\{p,q\} = \{7,3\}$, $\{6,3\}$, $\{5,3\}$, $\{7,4\}$, $\{6,4\}$, $\{5,4\}$ produced unphysical extrapolation behaviour. Moreover, potential energy functions with $q = 4$ require higher-order polynomial functions than did potential energy functions with $q = 3$ to obtain an equivalent value of $\overline{dd}$. One of the original objectives of this work was to generate a simpler and more compact potential energy function than Coxon's, while modelling all of the data accurately and obtaining a potential whose scattering length matched the value Chin *et al.* [4] determined. However, the latter objec-

tive required us to relax the preference to achieve compactness, and as a result, additional parameters are added to the potential energy function in order to make the extrapolation region of the potential consistent with theory.

To remove unnatural curvature from the extrapolation region of the potential seen in Fig. 3.4, the parameter q in our model was raised 5. As can be seen from Fig. 4.2, the $C_6^{\text{eff}}(r)$ and $C_8^{\text{eff}}(r)$ plots for our recommended potential deviate negligibly from the theoretical limiting slope of of C_8 and C_{10}, respectively. A less desirable effect of the use of $q = 5$ on the potential energy function is the need to increase the order of the exponent polynomial function in order to minimize $\overline{dd}$. The integer parameter q determines the range for which the y_q is defined on. This fundamental quality q has an indirect impact on the polynomial order of the potential N_β. Moreover, there is a loss in the quality of fit, such that there is an increase in the value of $\overline{dd}$. While it is important and desirable to minimize the number of potential parameters used when generating a potential energy function, it is of greater importance for the potential energy function to be as consistent as possible with experimental data *i.e.* to yield a minimum $\overline{dd}$. If a C_6 equal to $4.0\,\text{x}\,10^7$ is used, the minimal value of the dimensionless root mean square deviation $\overline{dd}_{\text{min}}$ that is associated with the potential where $C_6 = 4.0\,\text{x}\,10^7$ cm^{-1} Å^6 is 0.671229. The percent difference of the $\overline{dd}$ associated with chosen potential is:

$$\begin{aligned}\frac{\left|\overline{dd} - \overline{dd}_{\text{min}}\right|}{\overline{dd}_{\text{min}}}\,\text{x}\,100\% &= \frac{|0.673689 - 0.671229|}{0.671229}\,\text{x}\,100\% \\ &= 0.365\%\end{aligned}$$

Thus, the percent difference between the $\overline{dd}$ value used in the final fitted potential and the

fitted potential associated with $\overline{dd}_{\rm min}$ is quite small. Table 4.1 lists all of the parameters used to generate the potential energy function used in the analysis of $X\,^1\Sigma_g^+$ state of Cs_2.

The origin of the potential used in this analysis is rooted in the inability of preliminary potential energy functions with $q = 3, 4$ to extrapolate realistically from the outermost turning point of the last observed vibrational level to the dissociation limit. By setting $q = 5$, the resulting increase of $\overline{dd}$ is counteracted by increasing the polynomial order from $N_\beta = 17$ to $N_\beta = 22$. To obtain the desired scattering length by increasing or decreasing C_6 would mean moving further away from the minimal $\overline{dd}$. Fig. 4.2 shows the resulting $C_6^{\rm eff}(r)$ and $C_8^{\rm eff}(r)$ plots for the extrapolation region of the recommended MLR model for the $X\,^1\Sigma_g^+$ state of Cs_2. The potentials shown in section 3.2.1 use a different $u_{\rm LR}(r)$ form than the potential shown in Fig. 4.2. However, the potential energy function whose parameters are in Table 4.1 adheres to theory. Moreover, the $C_6^{\rm eff}(r)$ plots has a y-intercept of C_6 and a limiting slope equal to C_8. However, unlike the plots in Fig. 3.4 with $q = 3, 4$, the $C_8^{\rm eff}(r)$ plot in Fig. 4.2 not only exhibits a y-intercept of C_8, it also exhibits the correct limiting slope which is equal to C_{10}. Table 4.2 and 4.3 present the calculated energies G_υ for each of the 156 bound vibrational levels that define this potential.

Table 4.4 collects the highest three vibrational levels $\upsilon = 154, 155, 156$ and compares their binding energies to those calculated by Jeremy Hutson of Durham University, England, based on a molecular potential fit to the Feshbach resonances of Chin *et al.* [4]. Table 4.4 verifies that our highest vibrational levels are consistent with those determined using cold atom calculations. If the potential in this analysis did not impart the true scattering length, then reproducing the vibrational determined from cold atom calculations would have been highly improbable. Matching the binding energies in this analysis to those from cold

atom calculations offers an independent validation of the quality of the extrapolation of our empirical potentials.

A minimized value for $\overline{dd}$ indicates that the calculated vibrational levels inside the data region are accurate and thus, consistent with experiment. Plots of $C_6^{\text{eff}}(r)$ and $C_8^{\text{eff}}(r)$ indicate that extrapolation from the outermost turning point of the highest observed vibrational level $v = 136$ to the asymptotic limit $\mathfrak{D}_{\text{e}}$ adheres to the theoretical inverse power sum. Inclusion of the high quality PAS data measured by Danzl *et al.* [5] forces the potential to approach the desired "hyperfine-free" asymptotic limit. Finally, the comparison of the three highest vibrational levels calculated in this analysis to those calculated using cold atom calculations implies accuracy in the vibrational levels that are, in general, the most uncertain.

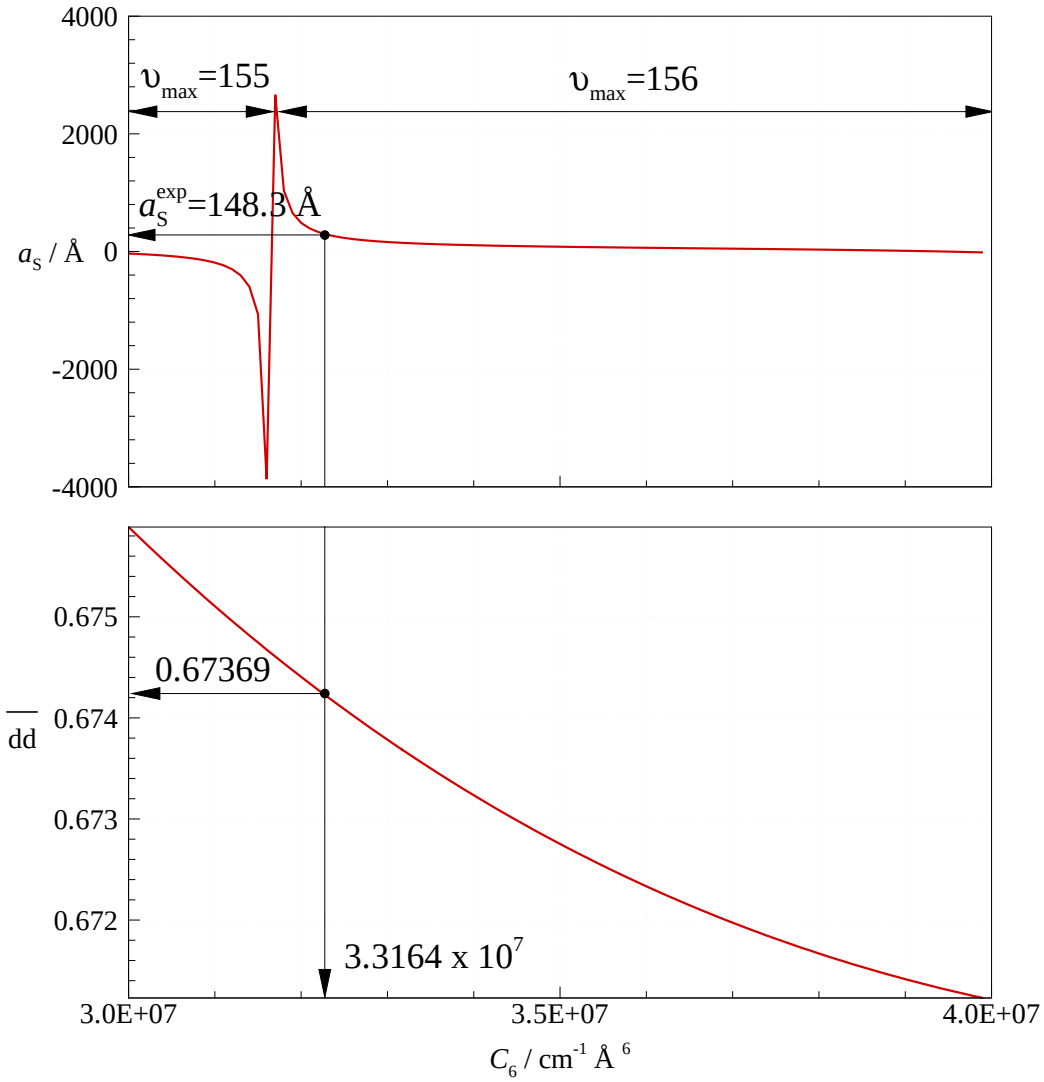

Figure 4.1: Plot of the scattering length a_S (top) and $\overline{dd}$ (bottom) as a function of C_6 for the $X\,^1\Sigma_g^+$ state of Cs_2 with $M3LR_{5,5}^{6,2}(22)$.

Table 4.1: Fit parameters used to generate the molecular potential for the $X\,^1\Sigma_g^+$ state.

Parameter	Value	Parameter	Value
β_0	$9.49905\,\mathrm{x}\,10^{-2}$	β_{19}	$1.175\,\mathrm{x}\,10^{2}$
β_1	$-3.72698\,\mathrm{x}\,10^{-1}$	β_{20}	$-7.5\,\mathrm{x}\,10^{1}$
β_2	$-4.090736\,\mathrm{x}\,10^{-2}$	β_{21}	$-3.67\,\mathrm{x}\,10^{1}$
β_3	$1.29657\,\mathrm{x}\,10^{-1}$	β_{22}	$1.3\,\mathrm{x}\,10^{1}$
β_4	$1.486696\,\mathrm{x}\,10^{-1}$	β_∞	0.9469102524695 *
β_5	$1.71395\,\mathrm{x}\,10^{-1}$	r_e/Å	4.647967771
β_6	$2.95883\,\mathrm{x}\,10^{-1}$	$\mathfrak{D}_\mathrm{e}/\mathrm{cm}^{-1}$	3650.041851
β_7	$5.47375\,\mathrm{x}\,10^{-1}$	$C_6/(10^7\ \mathrm{cm}^{-1}\ \mathrm{Å}^6)$	3.3164
β_8	-1.14615	$C_8/(10^9\ \mathrm{cm}^{-1}\ \mathrm{Å}^8)$	1.38
β_9	-2.7883	$C_{10}/(10^{10}\ \mathrm{cm}^{-1}\ \mathrm{Å}^{10})$	6.01
β_{10}	9.98557	$\mathrm{M_{Cs}}$/a.u.	132.905451933 [54]
β_{11}	$1.69149\,\mathrm{x}\,10^{1}$	r_ref/Å	6.2
β_{12}	$-4.17899\,\mathrm{x}\,10^{1}$	r_min/Å	3.0
β_{13}	$-5.76544\,\mathrm{x}\,10^{1}$	r_max/Å	99.5
β_{14}	$1.08881\,\mathrm{x}\,10^{2}$	Δr/Å	0.001
β_{15}	$1.24037\,\mathrm{x}\,10^{2}$	p	5
β_{16}	$-1.716\,\mathrm{x}\,10^{2}$	q	5
β_{17}	$-1.6159\,\mathrm{x}\,10^{2}$	ρ_AB	0.434
β_{18}	$1.5781\,\mathrm{x}\,10^{2}$	a_S/Å	148.3
		$\overline{dd}$	0.673689

* This parameter value is derived from others using Eq. (2.26)

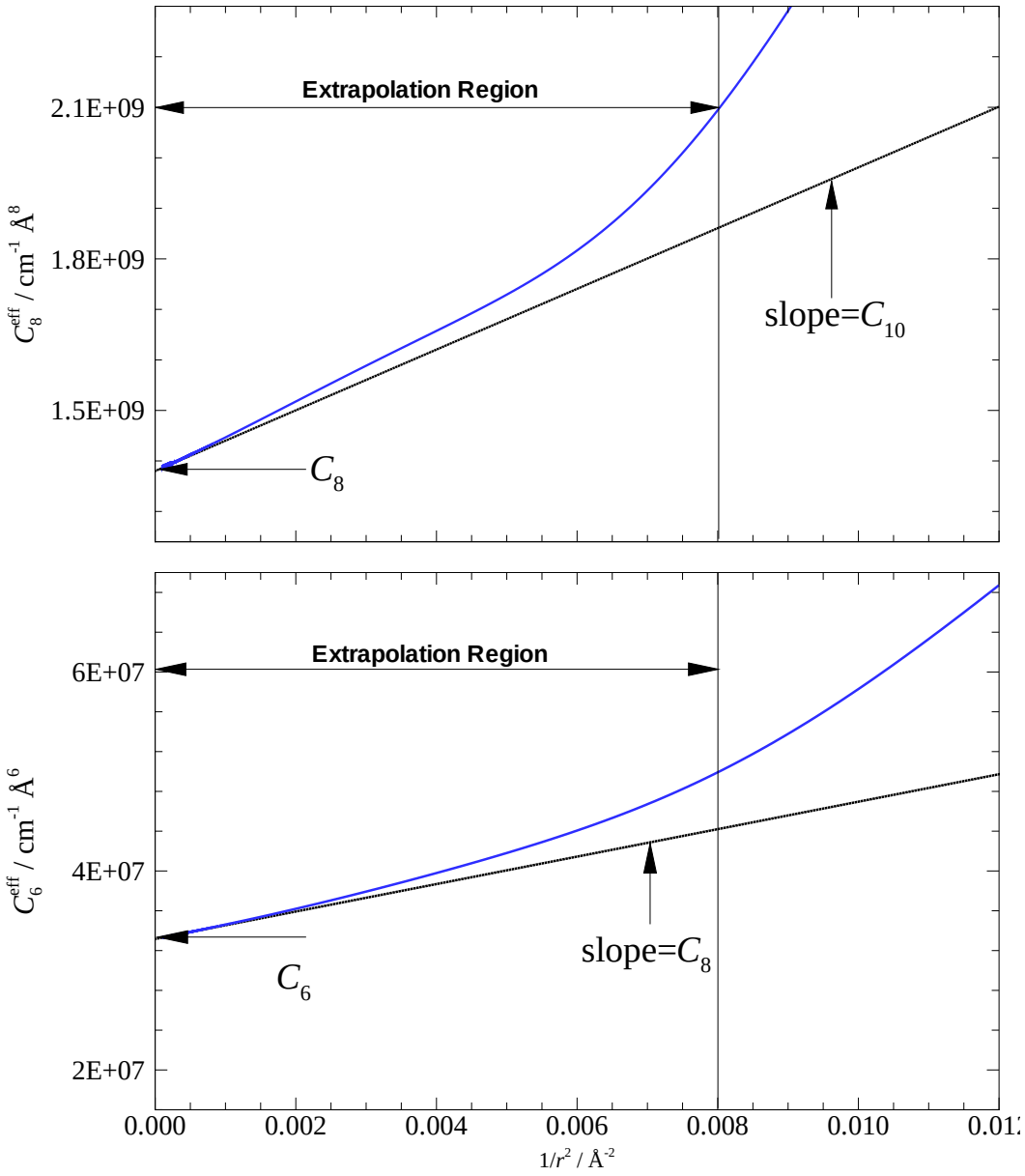

Figure 4.2: Plot of $C_6^{\text{eff}}(r)$ and $C_8^{\text{eff}}(r)$ as a function of $1/r^2$ for the $X\,^1\Sigma_g^+$ state of Cs_2 using the recommended $\text{M3LR}_{5,5}^{6,2}(22)$ in table 4.1.

Table 4.2: Vibrational energies for the $X\,^1\Sigma_g^+$ state of Cs_2 expressed relative to the dissociation limit for the recommended M3LR$^{6,2}_{5,5}$(22) potential of Table 4.1.

v	G_v / cm^{-1}	v	G_v / cm^{-1}	v	G_v / cm^{-1}	v	G_v / cm^{-1}
0	-3629.0599	20	-2823.9308	40	-2090.1202	60	-1436.6084
1	-3587.2046	21	-2785.4887	41	-2055.4438	61	-1406.2678
2	-3545.5140	22	-2747.2249	42	-2020.9685	62	-1376.1640
3	-3503.9886	23	-2709.1405	43	-1986.6957	63	-1346.2994
4	-3462.6290	24	-2671.2363	44	-1952.6269	64	-1316.6760
5	-3421.4359	25	-2633.5133	45	-1918.7636	65	-1287.2964
6	-3380.4096	26	-2595.9724	46	-1885.1074	66	-1258.1628
7	-3339.5510	27	-2558.6146	47	-1851.6598	67	-1229.2777
8	-3298.8605	28	-2521.4409	48	-1818.4224	68	-1200.6436
9	-3258.3387	29	-2484.4524	49	-1785.3969	69	-1172.2628
10	-3217.9863	30	-2447.6501	50	-1752.5849	70	-1144.1381
11	-3177.8040	31	-2411.0350	51	-1719.9882	71	-1116.2721
12	-3137.7924	32	-2374.6084	52	-1687.6085	72	-1088.6673
13	-3097.9522	33	-2338.3713	53	-1655.4477	73	-1061.3266
14	-3058.2840	34	-2302.3249	54	-1623.5075	74	-1034.2527
15	-3018.7887	35	-2266.4704	55	-1591.7899	75	-1007.4485
16	-2979.4669	36	-2230.8090	56	-1560.2967	76	-980.9168
17	-2940.3194	37	-2195.3420	57	-1529.0299	77	-954.6606
18	-2901.3471	38	-2160.0706	58	-1497.9916	78	-928.6829
19	-2862.5506	39	-2124.9963	59	-1467.1837	79	-902.9868

Table 4.3: Vibrational energies for the $X\,^1\Sigma_g^+$ state of Cs_2, expressed relative to the dissociation limit for the recommended M3LR$^{6,2}_{5,5}$(22) potential of Table 4.1 continued.

v	G_v / cm^{-1}	v	G_v / cm^{-1}	v	G_v / cm^{-1}	v	G_v / cm^{-1}
80	-877.5754	100	-434.4727	120	-137.3900	140	-12.2271
81	-852.4518	101	-415.8674	121	-126.9741	141	-10.0498
82	-827.6194	102	-397.6304	122	-117.0064	142	-8.1537
83	-803.0814	103	-379.7663	123	-107.4885	143	-6.5181
84	-778.8411	104	-362.2793	124	-98.4217	144	-5.1221
85	-754.9021	105	-345.1741	125	-89.8068	145	-3.9452
86	-731.2677	106	-328.4551	126	-81.6438	146	-2.9674
87	-707.9416	107	-312.1268	127	-73.9317	147	-2.1688
88	-684.9273	108	-296.1936	128	-66.6689	148	-1.5303
89	-662.2285	109	-280.6601	129	-59.8526	149	-1.0330
90	-639.8489	110	-265.5307	130	-53.4791	150	-0.65837771
91	-617.7923	111	-250.8098	131	-47.5432	151	-0.38835947
92	-596.0626	112	-236.5017	132	-42.0385	152	-0.20519699
93	-574.6637	113	-222.6108	133	-36.9572	153	-0.09152481
94	-553.5994	114	-209.1413	134	-32.2896	154	-0.03038252
95	-532.8740	115	-196.0973	135	-28.0246	155	-0.00524231
96	-512.4914	116	-183.4826	136	-24.1493	156	-0.00003238
97	-492.4557	117	-171.3011	137	-20.6489		
98	-472.7712	118	-159.5563	138	-17.5072		
99	-453.4421	119	-148.2516	139	-14.7063		

Table 4.4: Comparison of the highest vibrational energies of the fitted $X\,^1\Sigma_g^+$ state potential from this analysis with those calculated by Hutson.

v	G_v / cm^{-1}	G_v (Hutson) / cm^{-1}
154	-0.0303	-0.0303
155	-0.00524	-0.00524
156	-0.0000323	-0.0000323

Chapter 5

The $a\,^3\Sigma_u^+$ State of the Cesium Dimer

5.1 Previous Work on the $a\,^3\Sigma_u^+$ State of Cs_2

A recent DPF analysis of the $a\,^3\Sigma_u^+$ state of Cs_2 used the following modified version of the MLR potential energy function [7]:

$$V_{\rm MLR-Xie}(r) = V_\infty - \mathfrak{D}_{\rm e} + \mathfrak{D}_{\rm e}\left\{1 - \left[(1-a)\left(\frac{r_{\rm e}}{r}\right)^{N_\beta} + a\left(\frac{r_{\rm e}}{r}\right)^{M}\right] e^{-\beta(y)\cdot y_p^{\rm eq}(r)}\right\}^2 \qquad (5.1)$$

in which N_β is the inverse-power characterizing the leading term in the long-range tail of this potential, M is the inverse power associated with second longest-range term in the long-range potential, V_∞ is the absolute energy at the dissociation limit, and:

$$\beta(y) = \beta_0 + \beta_1 y + \beta_2 y^2 + \beta_3 y^3 + \cdots \qquad (5.2)$$

in which

$$y = \frac{r^p - r_e^p}{r^p + r_e^p} \tag{5.3}$$

As $r \to \infty$, $y \to 1$ such that $\beta(1)$ is equal to the sum of all β values in Eq. (5.2). The term $\beta(1)$ is analogous to β_∞ of Eq. (2.26), but the algebraic structure does not constrain Eq. (5.1) to adopt the correct long-range form without altering the β-parameters *ad hoc*. The Xie *et al.* potential analysis acknowledges that the theoretically predicted inverse-power sum is the correct representation of a molecular potential at long-range:

$$V_{\mathrm{MLR-Xie}}(r) \simeq V_\infty - \frac{C_N}{r^N} - \frac{C_M}{r^M} \tag{5.4}$$

in which $N = 6$ and $M = 8$. The authors quote the C_6 value from the work of Leo *et al.*, see Table 2.1, and a C_8 equal to $1.288\,\mathrm{x}\,10^9$ cm^{-1} Å^8 from a private communication with Bergeman and deMille. The authors show that the long-range coefficients in Eq. (5.4) may be expressed in terms of the non-physical β-parameters of their potential energy function:

$$C_6 = 2\,\mathfrak{D}_e\,(1-a)\exp\left(-\beta(1)\right)\,r_e^6 \tag{5.5}$$

and

$$C_8 = 2\,\mathfrak{D}_e\,a\exp\left(-\beta(1)\right)\,r_e^8 \tag{5.6}$$

However, the values of C_6 and C_8 that they present from literature and a personal communication do not match the values that Eq. (5.5) and (5.6) yield from the parameter values published for their potential, which are $3.748\,\mathrm{x}\,10^7$ cm^{-1} Å^6 and $1.452\,\mathrm{x}\,10^9$ cm^{-1} Å^8, respectively. That is to say, the first and second leading dispersion coefficients that Xie *et al.*

calculate from their potential parameters do not agree with the theoretical values they claim to be emulating. Furthermore, the empirical C_6 and C_8 from the work of Xie *et al.* differ in magnitude greatly from all of the various values that are in the literature and collected in Table 2.1.

Xie *et al.* fitted their modified version of the MLR to term values they derived from fluorescence series transitions they observed from experiment. They do not present a quantitative measure to indicate how well the calculated potential represents the experimental data. Their modification to the MLR potential is counterintuitive because they relinquish the ability to constrain C_6 and C_8 to match theoretical values, which are often much more accurate than any values that may be obtained empirically. Modifications to a potential energy function should provide global improvement to the function's ability to fit to experimental data, or the function's ability to extrapolate from $\upsilon_{\max}$ to the asymptotic limit. Furthermore, analytic potential energy functions should be able to represent many different species and electronic states. Since there is no provision of a residual, their potential energy function cannot be said to improve or diminish the quality of fit relative to the MLR. The innovative feature of Eq. (2.22) is the introduction of β_∞ because it insures that the potential energy function is the appropriate inverse-power sum at long-range. By explicitly removing β_∞, the potential energy function of Xie *et al.* cannot be guaranteed to exhibit the correct theoretical behaviour as it approaches the asymptotic limit. While this potential energy function may have utility for the authors, it does not offer coherent control of the extrapolation region, and it was not been shown to offer an improved ability to represent experimental data.

5.2 Fitting Results and Analysis

Xie *et al.* determined term values from the fluorescence transitions they observed from experiment, which they fitted Eq. (5.1) to. They used the ground singlet state $\mathfrak{D}_e$ value observed by Danzl *et al.* [5] as their V_∞ in Eq. (5.1). In this analysis the term values were expressed relative to the hyperfine-free limit of 3650.0449 cm^{-1}, see Section 4.2, from the singlet state to insure that the triplet state went to the same asymptotic limit as the singlet state, and to allow the term values to be treated as photoassociation data.

As mentioned previously, the $X\,^1\Sigma_g^+$ and $a\,^3\Sigma_u^+$ states of Cs_2 approach the same asymptotic limit, dissociating to identical ground-state atoms, and have identical inverse-power long-range functions that describe the behaviour of these diatomic potentials as they approach the asymptotic limit. Chapter 4 described the technique by which an accurate potential energy function was generated in this work for the $X\,^1\Sigma_g^+$ of Cs_2. Moreover, the technique used to generate a molecular potential that would impart a scattering length that is in agreement with experiment was dependent on the numerical value of the dispersion coefficient that corresponds to the leading term of the long-range function. To coherently describe the long-range of both molecular states simultaneously, the very same form of u_{LR} must be used for the triplet state. A significant consequence of this is the inherent inability to vary the long-range coefficients for the $a\,^3\Sigma_u^+$ state.

In Fig. 5.1, the scattering length and $\overline{dd}$ are plotted as a function of r_{ref}. As the value of r_{ref} is increased from 7.0 $\mathring{A}$ to larger values, the scattering length gets increasingly larger until a scattering length of infinite magnitude is acheived. The desired scattering length is 1273 Å, thus the desired r_{ref} value is found to be smaller than the r_{ref} value that corresponds

to the singularity. Fig. 5.1 shows that using $r_{\rm ref} = 8.7005\,\text{Å}$ allows the molecular potential to have a scattering length of $a_{\rm T}$ of 1273 Å thus, matching the value of Chin *et al.* [4]. The non-physical parameter $r_{\rm ref}$ is the centre for the radial expansion variable of Eq. (2.25). The value chosen for $r_{\rm ref}$ is shown to be of consequence to the molecular potential's ability to represent the experimental data set with a modest number of parameters. In particular, there usually exists a value of $r_{\rm ref}$ that will minimize the $\overline{dd}$ value that corresponds to a given potential and its corresponding potential parameters. For a given experimental datum, the molecular potential should be able to impart a calculated value that is within the experimental uncertainty. That is to say, when the difference is taken between the experimental and calculated values, its absolute value should not exceed that of the experimental uncertainty. The uncertainty on each of the 1440 term values that are treated as binding energies is 0.2 cm^{-1}. The final fitted potential used $r_{\rm ref} = 8.7005\,\text{Å}$, which has a $\overline{dd}$ value of 1.41784. This implies that on average the calculated values are outside the experimental uncertainties. The minimum value of the dimensionless root mean square deviation $\overline{dd}_{\rm min}$ is obtained when $r_{\rm ref} = 9.1\,\text{Å}$, $p = q = 5$, $N_\beta = 4$, and is 1.41736. The percent difference is given by:

$$\begin{aligned} \frac{\left|\overline{dd} - \overline{dd}_{\rm min}\right|}{\overline{dd}_{\rm min}} \,\text{x}\, 100\% &= \frac{|1.41784 - 1.41736|}{1.41736} \,\text{x}\, 100\% \\ &= 0.0339\% \end{aligned}$$

Thus, the $\overline{dd}$ value associated with the final fitted potential is within 0.0339% of the most optimal fitted potential. This percent difference indicates that the fitted potential that imparts a scattering length that is in agreement with experiment does not result in a sig-

nificant decrease in the overall fit quality. Tests showed that for the $X\,^1\Sigma_g^+$ state that our MLR model potentials require q to equal 5 to insure the extrapolation region adheres to the proper behaviour dictated by theory. For the $a\,^3\Sigma_u^+$ state of Cs_2, the quality of fit was equivalent for $q = 3$, $q = 4$, and $q = 5$ for a given N_β, so it was convenient to simply use $q = 5$ for this potential energy model since it was also used for the singlet state. The $a\,^3\Sigma_u^+$ state adheres to the correct limiting behaviour when $q = 5$. Fig. 5.2 shows $C_m^{\rm eff}$ for $m = 6, 8$. However, the $C_8^{\rm eff}$ plot does show changes in curvature midway between the asymptotic limit and $1/r^2 = 0.006$. This change in curvature is unphysical because the curvature should be positive due to the next leading term in the $u_{\rm LR}(r)$ being a positive C_{10}. The potential for the singlet state uses the same form for $u_{\rm LR}(r)$ and it yields the correct scattering length, has a small $\overline{dd}$, $C_m^{\rm eff}$ plots that agree with theory, and the calculated values for the three highest vibrational levels agree with the vibrational levels calculated from the independent analysis of Hutson. Given the result for the singlet state, it seems the dispersion part of the potential is not the cause of this unphysical behaviour, but rather, it is perhaps due to the absolute placement of the term values. The potential parameters for the final fitted potential determined from the present analysis for the $a\,^3\Sigma_u^+$ state of Cs_2 are presented in Table 5.1.

Table 5.2 lists the calculated level energies of the final fitted potential of the $a\,^3\Sigma_u^+$ state of Cs_2. Table 5.3 lists the binding energies for the three highest vibrational levels, and the binding energies attributed to the three highest calculated vibrational levels associated with a potential energy function that was fitted to the Feshbach resonances of Chin *et al.* [4], derived by Jeremy Hutson of Durham University, England [9]. The values from the fitted potential in this analysis are in excellent agreement with those determined by Hutson [9]. Varying the $r_{\rm ref}$ parameter to obtain a potential whose scattering length agrees with

the experimental value necessarily moves the highest vibrational levels of this molecular potential. This is, of course, analogous to varying the value of C_6 coefficient to obtain a scattering length for the $X\,^1\Sigma_g^+$ state that matches experiment. However, the noteworthy difference in varying $r_{\rm ref}$ for the $a\,^3\Sigma_u^+$ state is the unpredictable and oscillatory variation of the fitted well-depth $\mathfrak{D}_{\rm e}$ as shown in Fig. 5.3.

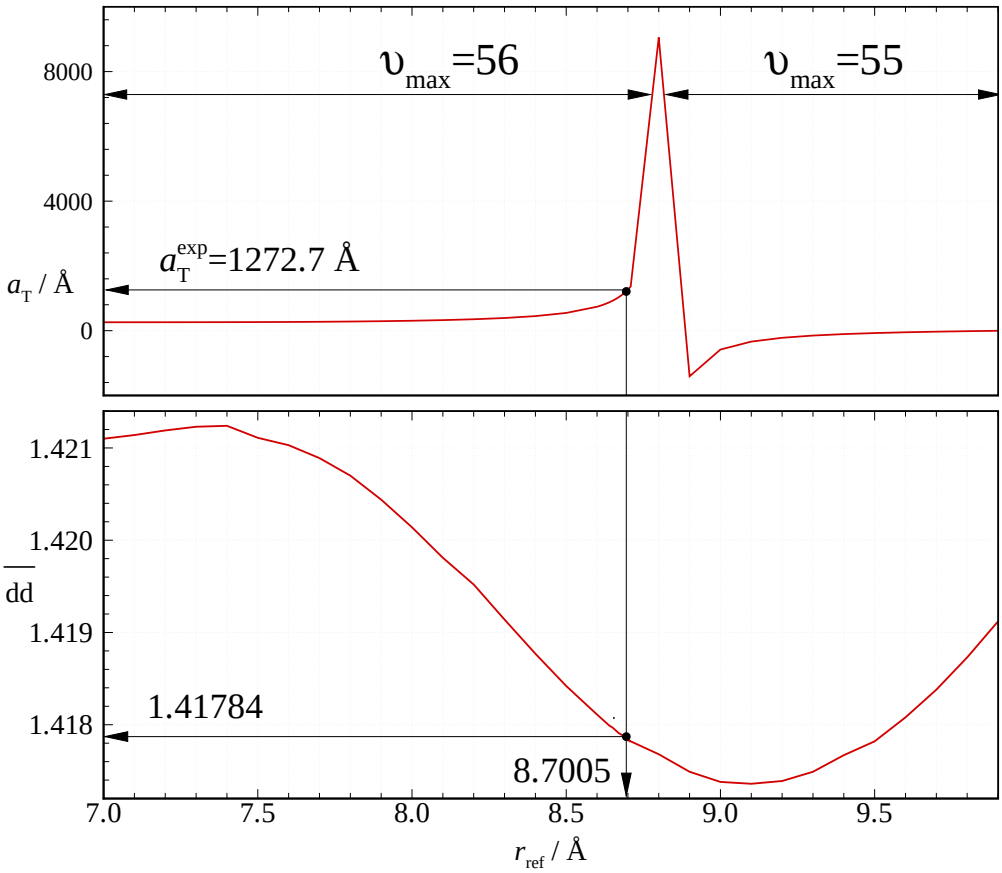

Figure 5.1: Plot of the scattering length a_T (top) and $\overline{dd}$ (bottom) as a function of r_{ref} for the $a\,^3\Sigma_u^+$ state of Cs_2 with $M3LR_{5,5}^{ref}(3)$.

Table 5.1: Fit parameters used to generate the molecular potential for the $a\,^3\Sigma_u^+$ state.

Parameter	Value	Parameter	Value
β_0	-4.324429443667 x 10^{-1}	M_{Cs}/a.u.	132.905451933 [54]
β_1	-9.206933982533 x 10^{-2}	r_{ref}/Å	8.7005
β_2	-6.845846740405 x 10^{-2}	r_{min}/Å	3.0
β_3	-1.308218973148 x 10^{-2}	r_{max}/Å	99.5
β_4	3.457944786933 x 10^{-1}	Δr/Å	0.001
β_∞	-3.971077022867 x 10^{-1}	p	5
r_e/Å	6.226182057299	q	5
$\mathfrak{D}_e$/cm^{-1}	279.2222367314	ρ_{AB}	0.434
$C_6/(10^7$ cm^{-1} Å$^6)$	3.3164	a_T/Å	1273
$C_8/(10^9$ cm^{-1} Å$^8)$	1.38	$\overline{dd}$	1.41784
$C_{10}/(10^{10}$ cm^{-1} Å$^{10})$	6.01		

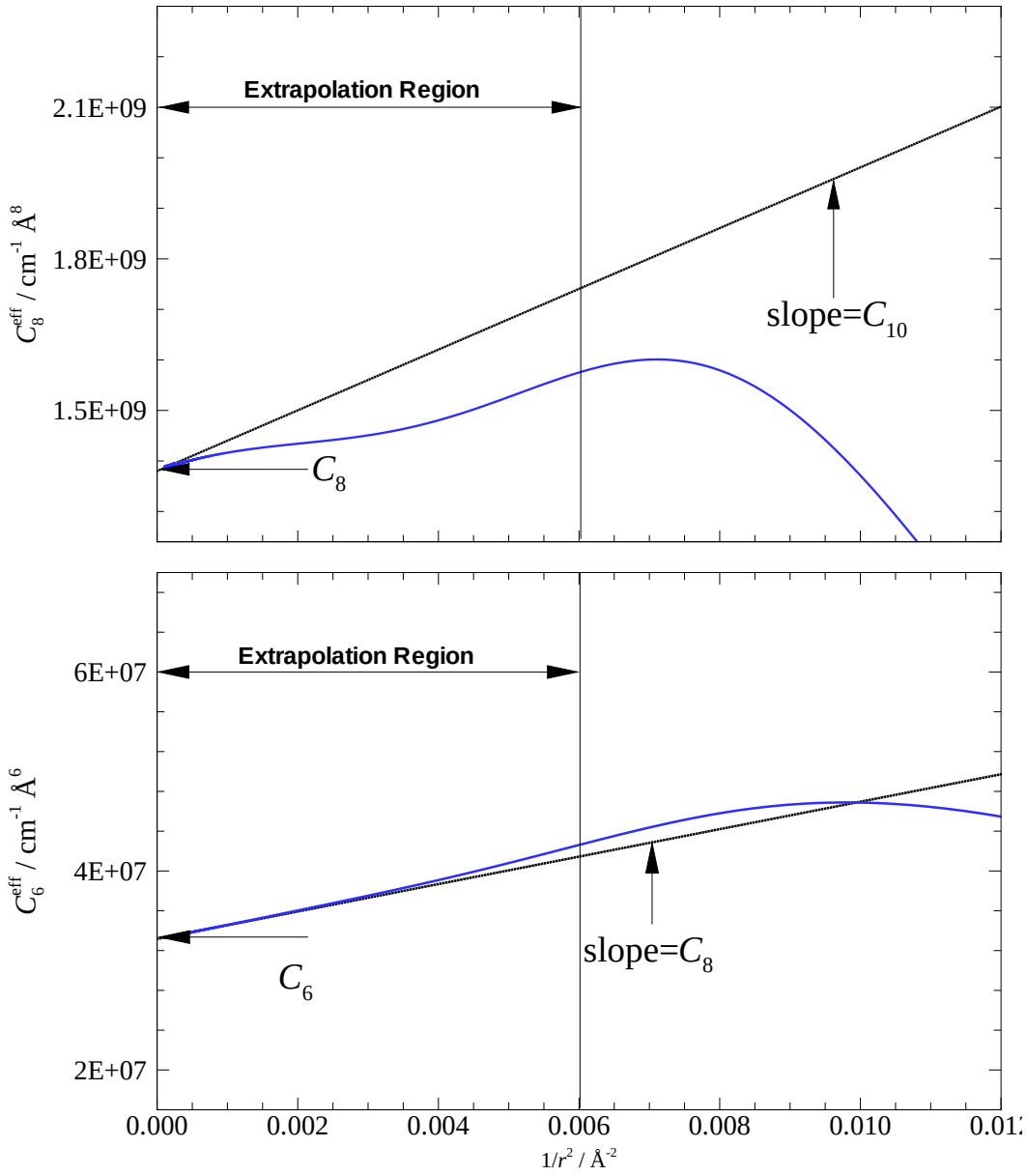

Figure 5.2: Plot of $C_6^{\text{eff}}(r)$ and $C_8^{\text{eff}}(r)$ as a function of $1/r^2$ for the $a\,^3\Sigma_u^+$ state of Cs_2 with $\text{M3LR}_{5,5}^{8.7005}(3)$.

Table 5.2: Vibrational energies for the $a\,^3\Sigma_u^+$ state of Cs_2 for the recommended $M3LR_{5,5}^{8.7005}(3)$ potential of Table 5.1.

v	G_v / cm^{-1}	v	G_v / cm^{-1}	v	G_v / cm^{-1}
0	-273.5056	20	-95.2092	40	-10.7899
1	-262.3059	21	-88.7564	41	-8.9566
2	-251.3769	22	-82.5423	42	-7.3305
3	-240.7067	23	-76.5669	43	-5.9043
4	-230.2862	24	-70.8299	44	-4.6690
5	-220.1079	25	-65.3306	45	-3.6143
6	-210.1664	26	-60.0685	46	-2.7284
7	-200.4577	27	-55.0426	47	-1.9987
8	-190.9792	28	-50.2522	48	-1.4111
9	-181.7294	29	-45.6962	49	-0.95111378
10	-172.7076	30	-41.3738	50	-0.60362557
11	-163.9139	31	-37.2843	51	-0.35309399
12	-155.3490	32	-33.4267	52	-0.18375471
13	-147.0138	33	-29.8003	53	-0.07970205
14	-138.9096	34	-26.4044	54	-0.02497799
15	-131.0377	35	-23.2379	55	-0.00366536
16	-123.3996	36	-20.2997	56	-0.00000017621776
17	-115.9966	37	-17.5882		
18	-108.8299	38	-15.1015		
19	-101.9005	39	-12.8366		

Table 5.3: Comparison of the highest vibrational energies of the fitted $a\,^3\Sigma_u^+$ state potential from this analysis with those calculated by Hutson.

v	G_v / cm^{-1}	G_v (Hutson) / cm^{-1}
54	-0.0249	-0.0249
55	-0.00366	-0.00366
56	-0.000000176	-0.000000171

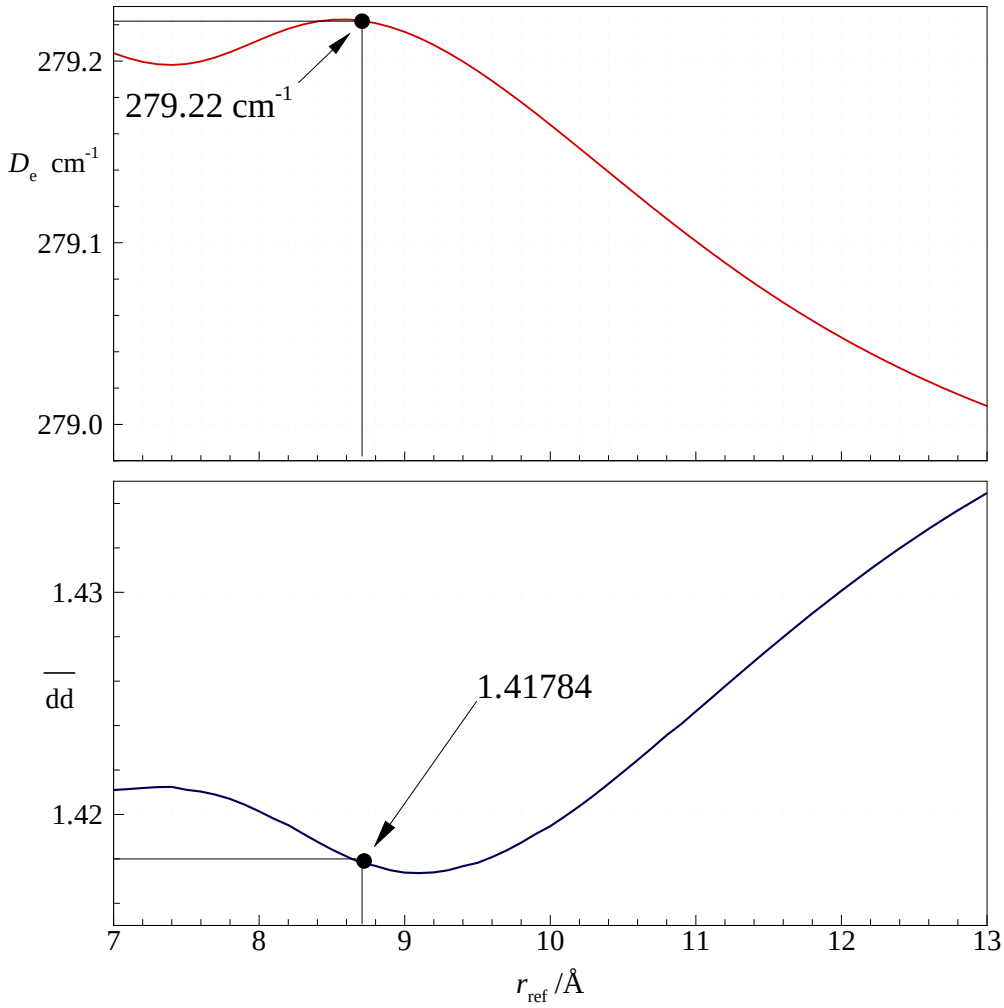

Figure 5.3: Plot of $\mathfrak{D}_e$ and $\overline{dd}$ as a function of r_{ref} for the $a\,^3\Sigma_u^+$ state of Cs_2.

Chapter 6

Summary

New potential energy functions have been developed for the $a\,^3\Sigma_u^+$ and $X\,^1\Sigma_g^+$ states of Cs_2. The long-range tails for both electronic states have been modelled to consist of sums of inverse-power terms from theory. The extrapolation behaviour of these potentials were examined using the $C_m^{\rm eff}$ plots of Figs. 4.2 and 5.2. On a $C_m^{\rm eff}$ plot, the fitted potential curve is predicted from theory to approach a y-intercept of C_m and have a slope equal to the next leading dispersion coefficient in the inverse-power sum. For the triplet state, this requirement was met only when q in Eq. (2.25) was equal to 5. The use of $q = 5$ necessitates incorporating a higher-order polynomial in Eq. (2.24) than would be necessary to obtain an equivalent quality of fit using $q < 5$.

It has been shown that including the theoretical exchange energy function used by Vanhaecke *et al.* [3] for Cs_2 in the MLR potential energy function is both unnecessary and impossible. The theoretical exchange energy function proved to be unnecessary when the fitted potential energy curves from the triplet and singlet states were used in Eq. (3.10) to

verify that the extrapolation regions of the two respective states agree with the theoretical exchange function. Fig. 3.12 shows that our two MLR potential energy functions effectively incorporate the theoretical exchange energy function as long as $u_{\rm LR}(r)$ includes at least the first three inverse-power terms predicted from theory. The MLR β_∞ parameter is defined by a logarithmic term that includes the value of $u_{\rm LR}(r)$ at $r = r_{\rm e}$. Consequently, Eq. (2.26) requires that $0 < u_{\rm LR}(r)$ for it to be defined. For the triplet state, the theoretical exchange is a large negative value at $r = r_{\rm e}$ that makes $u_{\rm LR}(r_{\rm e}) < 0$, which makes it impossible to define Eq. (2.26), and thus, the MLR potential energy function.

The extrapolation region of our $a\,^3\Sigma_u^+$ and $X\,^1\Sigma_g^+$ potentials for Cs_2 can be further examined by comparing the scattering length of the recommended molecular potential to their respective experimental values. The structure of the outer-wall of a molecular potential was shown to be very sensitive to the leading dispersion coefficient C_6, and the non-physical parameter $r_{\rm ref}$ that defines the dimensionless radial variable of Eq. (2.25). Variation of the C_6 coefficient for the singlet state allowed the scattering length of the MLR potential in table 4.1 to match the experimental value of Chin *et al.* [4]. Determining an accurate potential well for the singlet state in the well region and near the asymptotic limit by matching the scattering length of the calculated potential to the experimental value provides confidence in the chosen parameters. The same dispersion coefficients used to define $u_{\rm LR}(r)$ of the singlet state were used to define $u_{\rm LR}(r)$ of the triplet state. The radial variable expansion centre $r_{\rm ref}$ was the only other parameter available for varying the well capacity of the triplet state potential energy function such that the final potential could yield a scattering length that matched the experimental value.

In a private communication with Jeremy Hutson of Durham University, England, calcu-

lated vibrational levels were provided for the three highest bound vibrational levels for the $a\,^3\Sigma_u^+$ and $X\,^1\Sigma_g^+$ states of Cs_2. These vibrational levels were not given absolute quantum number labels, but Tables 4.4 and 5.3 show that they are in close agreement with the vibrational levels that correspond to $v = 156$, 155, and 154 for the singlet state and $v = 56$, 55, and 54 for the triplet state. The molecular potentials determined by Hutson are derived from cold-atom physics calculations, and use the Feshbach resonance data observed by Chin *et al.* [4]. The molecular potentials described in sections 4.2 and 5.2 were derived using direct potential fits to the fluorescence series and photoassociation data of the singlet state, and the reported term values of the triplet state. Therefore, the observed agreement in the two analyses in Tables 4.4 and 5.3 can be seen as two independent results, giving validity to the binding energies of these vibrational levels.

A shortcoming of the molecular potential determined in sections 4.2 and 5.2 are that the fits to spectroscopic data were not really optimal. That is to say, the values of $\overline{dd}$ for both electronic states are not minimized. In particular, Figs. 4.1 and 5.1 clearly show that the respective C_6 and $r_{\rm ref}$ values chosen for the singlet and triplet states are not coincident with the minima of $\overline{dd}$. While the very highest vibrational levels agree well with the independent predictions of Hutson, the levels that are slightly more strongly bound at the beginning of the extrapolation region could be inaccurate as there is no analogous way of determining the binding energies. It is conceivable that the inclusion of the higher-order dispersion coefficients could contribute to a greater level of accuracy at the beginning of the extrapolation region. If the inverse-power sum is incongruent with the highest observed vibrational levels, it can lead to larger residuals and thus, a larger value for $\overline{dd}$.

Future outlook on diatomic molecules should include the use of high-resolution PAS

data if it is available. Examples of systems of interest include the the rubidium dimer, and heternuclear diatomic molecules like rubidium cesium and potassium cesium. If PAS data is unavailable, analyses of diatomic potentials should focus on ensuring that the dissociation limit is held fixed using an alternative approach. This can be achieved by determining an accurate dissociation energy using some other computational method, and then holding the dissociation energy fixed during the potential fit. By fixing the dissociation limit and, by matching the scattering length with an accurate experimental value, the highest vibrational levels can be determined with accuracy without being spectroscopically observed.

Appendix

I DPotFit Input

I.1 $X\,^1\Sigma_g^+$ State of Cs_2

```
 55  55  0  1  1
 'revdataCoxon.4'

'iround_33164000'

 0.003  1  -2  0  5  0
 133 133
 'X0'  0  0  155  300  0
 2 0.0d0 0 20
 3.0  99.5  0.0010
 3 0.434d0  -2  1
 6   33164000                        1
```

```
8   1.38D+09                   1
10  6.01D+10                   1
3650.0449d0          0
4.647972d0           0

 22  22  5  5     6.200000000000D+00
 9.567420826492D-02  0
-3.567866384433D-01  0
-2.377652483493D-02  0
 1.466734317858D-01  0
 1.609387591733D-01  0
 2.300492780357D-01  0
 4.859674345663D-01  0
-7.669309796208D-02  0
-3.291589176137D+00  0
 2.952740674404D+00  0
 2.563198939463D+01  0
-1.292719803845D+01  0
-1.104063728957D+02  0
 3.797179900595D+01  0
 2.992441977465D+02  0
-6.554504343300D+01  0
-5.068466637544D+02  0
```

```
 6.566623853793D+01  0
 5.222080116442D+02  0
-3.349799200872D+01  0
-2.983092408679D+02  0
 6.220033634041D+00  0
 7.229612913783D+01  0

-1 -1    5  3  -1.000D+00   2.200D+00
-1 -1    3  3
```

I.2 $a\,^3\Sigma_u^+$ State of Cs_2

```
55  55  0  1  1
 'data_danzl.4'
 '8_7005'
 0.2  1  0  0  5  0
133 133
 'a1'  0  0  50  48   0
 2 0.0d0 0 20
 3.0  99.5  0.0010
 3 0.434d0  -2  1
 6 33164000           1
 8 1.38D+09           1
10 6.01D+10           1
```

```
 279.349d0           0
 6.23540d0           0

 4  4    5  5   8.7005D+00
-4.142960251327D-01  0
-1.431708097381D-01  0
 2.407722980732D-01  0
-3.688917032456D-01  0
-5.097715765462D-01  0

-1 -1    5  3  -1.000D+00   2.200D+00

-1 -1    3  3
```

II LEVEL Input

II.1 $X\,^1\Sigma_g^+$ State of Cs_2

```
 55 133  55 133  0   1
' Level test using Cs2 data '
 0.00001  0.5d0  1.0d0 1.0d0  1.d-08
-1 0  0   0.d0
```

```
 4       5 5   22  22 -0
  3.650041851127D+03  4.647967775597D+00  6.200000000000D+00

 3  -2  1  0.434d0

6   3.316400000000D+07 8   1.380000000000D+09 10   6.010000000000D+10

  9.499051111491D-02
 -3.726981674982D-01
 -4.090806023496D-02
  1.296392919089D-01
  1.486895184395D-01
  1.720230882839D-01
  2.957077951625D-01
  5.376539536162D-01
 -1.147130576653D+00
 -2.708427676798D+00
  1.001316741585D+01
  1.652892997773D+01
 -4.199122951214D+01
 -5.650348519869D+01
  1.096312550177D+02
```

```
 1.218986666297D+02
-1.732018584113D+02
-1.591845470976D+02
 1.597880613068D+02
 1.160039628294D+02
-7.631357364144D+01
-3.630597053826D+01
 1.336289024969D+01

 1 0  0  0  0 1  -1  0
 0 0 0
```

II.2 $a\,^3\Sigma_u^+$ State of Cs_2

```
 55 133  55 133  0   1
' Level test using Cs2 data '
 0.00001  0.5d0  1.0d0 1.0d0  1.d-08
-1 0  0   0.d0



 4       5 5    4   4 -0
  2.792222367314D+02  6.226182057299D+00  8.700500000000D+00

 3  -2  1  0.434d0
```

```
6   3.316400000000D+07 8   1.380000000000D+09 10   6.010000000000D+10

 -4.324429443667D-01
 -9.206933982533D-02
 -6.845846740405D-02
 -1.308218973148D-02
  3.457944786933D-01

 1 0  0  0  0 1  -1  0
 0 0 0
```

Bibliography

[1] R. J. Le Roy, 64^{th} Ohio State University International Symposium on Molecular Spectroscopy (Columbus, Ohio, 2009), paper MI-08.

[2] J. A. Coxon and P. G. Hajigeorgiou, J. Chem. Phys. **132**, 094105 (2010).

[3] N. Vanhaecke, C. Lisdat, B. T'Jampens, D. Comparat, A. Crubellier, and P. Pillet, Eur. Phys. J. D **28**, 351 (2004).

[4] C. Chin, V. Vuletić, A. J. Kerman, S. Chu, E. Tiesinga, P. J. Leo, and C. J. Williams, Phys. Rev. A **70**, 032701 (2004).

[5] J. G. Danzl, E. Haller, M. Gustavsson, M. J. Mark, R. Hart, N. Bouloufa, O. Dulieu, H. Ritsch, and H.-C. Nägerl, Science **321**, 1062 (2008).

[6] C. Amiot and O. Dulieu, J. Chem. Phys. **117**, 5155 (2002).

[7] F. Xie, V. B. Sovkov, A. M. Lyyra, D. Li, S. Ingram, J. Bai, V. S. Ivanov, S. Magnier, and L. Li, J. Chem. Phys. **130**, 051102 (2009).

[8] W. Weickenmeier, U. Deimer, M. Wahl, M. Raab, W. Demtröder, and W. Müller, J. Chem. Phys. **82**, 5354 (1985).

[9] J. Hutson, personal communication (7 October 2010).

[10] H. Margenau, Rev. Mod. Phys. **11**, 1 (1939).

[11] M. Marinescu, H. R. Sadeghpour, and A. Dalgarno, Phys. Rev. A **49**, 982 (1994).

[12] S. H. Patil and K. T. Tang, J. Chem. Phys. **106**, 2298 (1997).

[13] S. H. Patil and K. T. Tang, Chem. Phys. Lett. **301**, 64 (1999).

[14] A. Derevianko, W. R. Johnson, M. S. Safronova, and J. F. Babb, Phys. Rev. Lett. **82**, 3589 (1999).

[15] S. Kotochigova, E. Tiesinga, and P. Julienne, Phys. Rev. A **63**, 012517 (2000).

[16] P. Leo, C. Williams, and P. Julienne, Phys. Rev. **85**, 2721 (2000).

[17] C. Drag, B. Tolra, B. T'Jampens, D. Comparat, M. Allegrini, A. Crubellier, and P. Pillet, Phys. Rev. **85**, 1408 (2000).

[18] S. G. Porsev and A. Derevianko, J. Chem. Phys. **119**, 844 (2003).

[19] J. Hutson, personal communication (30 January 2012).

[20] J. Mitroy, personal communication (6 March 2012).

[21] J. A. Coxon, J. Mol. Spectrosc. **133**, 96 (1989).

[22] a) J. M. Hutson, J. Phys. B. (At. Mol. Phys.) **14**, 851–857 (1981); b) J. M. Hutson, QCPE Bulletin, **2**, no. 2, Program #435, Quantum Chemistry Program Exchange, Indiana University, Bloomington, Indiana.

[23] Y. Huang and R. J. Le Roy, J. Chem. Phys. **119**, 7398 (2003).

[24] A. Shayesteh, R. D. E. Henderson, R. J. Le Roy, and P. F. Bernath, J. Phys. Chem. A **111**, 12495 (2007).

[25] R. Le Roy and J. van Kranendonk, J. Chem. Phys. **61**, 4750 (1974).

[26] R. J. Le Roy, *Determining Equilibrium Structures and Potential Energy Functions for Diatomic Molecules*, Chapter 6, pp. 168-211, of *Equilibrium Structures of Molecules*, J. Demaison and A. G. Csaszar editors, Taylor & Francis, London (2010).

[27] R. Rydberg, Z. Physik **73**, 376 (1932).

[28] J. L. Dunham, Phys. Rev. **41**, 713-720 (1932); *ibid* **41**, 721-731 (1932).

[29] J. F. Ogilvie, Proc. Roy. Soc. (London) **A 378**, 287 (1981).

[30] J. F. Ogilvie, J. Chem. Phys. **88**, 2804 (1988).

[31] A. A. Šurkus, R. J. Rakauskas, and A. B. Bolotin, Chem. Phys. Lett. **105**, 291 (1984).

[32] R. J. Le Roy, N. Dattani, J. A. Coxon, A. J. Ross, P. Crozet, and C. Linton, J. Chem. Phys. **131**, 204309 (2009).

[33] C. Samuelis, E. Tiesinga, T. Laue, M. Elbs, H. Knöckel, and E. Tiemann, Phys. Rev. A **63**, 012710 (2000).

[34] J. A. Coxon and P. G. Hajigeorgiou, 49^{th} Ohio State University International Symposium on Molecular Spectroscopy (Columbus, Ohio, 1994), paper WE05.

[35] E. G. Lee, J. Y. Seto, T. Hirao, P. F. Bernath, and R. J. Le Roy, J. Mol. Spectrosc. **194**, 197 (1999).

[36] J. Y. Seto, R. J. Le Roy, J. Vergès, and C. Amiot, J. Chem. Phys. **113**, 3067 (2000).

[37] R. J. Le Roy, D. R. T. Appadoo, K. Anderson, A. Shayesteh, I. E. Gordon, and P. F. Bernath, J. Chem. Phys. **123**, 204304 (2005).

[38] J. Y. Seto, Z. Morbi, F. Charron, S. K. Lee, P. F. Bernath, and R. J. Le Roy, J. Chem. Phys. **110**, 11756 (1999).

[39] E. Tiemann, Z. Phys. D – Atoms, Molecules and Clusters **5**, 77 (1987).

[40] U. Wolf and E. Tiemann, Chem. Phys. Lett. **133**, 116 (1987).

[41] U. Wolf and E. Tiemann, Chem. Phys. Lett. **139**, 191 (1987).

[42] E. Tiemann, Mol. Phys. **65**, 359 (1988).

[43] A. Pashov, W. Jastrzębski, and P. Kowalczyk, Comp. Phys. Comm. **128**, 622 (2000).

[44] A. Pashov, W. Jastrzębski, and P. Kowalczyk, J. Chem. Phys. **113**, 6624 (2000).

[45] A. Pashov, W. Jastrzębski, W. Jaśniecki, V. Bednarska, and P. Kowalczyk, J. Mol. Spectrosc. **203**, 264 (2000).

[46] R. J. Le Roy and R. D. E. Henderson, Mol. Phys. **105**, 663 (2007).

[47] R. J. Le Roy, C. C. Haugen, J. Tao, and H. Li, Mol. Phys. **109**, 435 (2011).

[48] M. Raab, G. Höning, W. Demtröder, and C. Vidal, J. Chem. Phys. **76**, 4370 (1982).

[49] G. Höning, M. Czajkowski, M. Stock, and W. Demtröder, J. Chem. Phys. **71**, 2138 (1979).

[50] O. Klein, Z. Physik **76**, 226 (1932).

[51] R. Rydberg, Z. Physik **80**, 514 (1933).

[52] A. L. G. Rees, Proc. Phys. Soc. (London) **59**, 998 (1947).

[53] P. Roman, Advanced Quantum Theory: An Outline of the Fundamental Ideas (Addison-Wesley, Reading, MA, 1965).

[54] A. Wapstra, G. Audi, and C. Thibault, Nucl. Phys. A **729**, 129 (2003).